Journal of Volcanology and Geothermal Research 464 (2025) 108346

Contents lists available at ScienceDirect

Journal of Volcanology and Geothermal Research

journal homepage: www.journals.elsevier.com/journal-of-volcanology-and-geothermal-research

Constraining the timing and climate forcing of the Long Island (Papua New Guinea) and Tarumae (Japan) eruptions and other 17th century volcanic eruptions

Imogen Gabriel [a,b,*], Helen M. Innes [c], Peter M. Abbott [a,b], Jörg Franke [b,d], Melanie Behrens [e], Nathan J. Chellman [f], Maria Hörhold [e], William Hutchison [c], Joseph R. McConnell [f], Birthe Twarloh [e], Michael Sigl [a,b,*]

[a] Climate and Environmental Physics, Physics Institute, University of Bern, Bern, Switzerland
[b] Oeschger Centre for Climate Change Research, University of Bern, Bern, Switzerland
[c] School of Earth and Environmental Sciences, University of St Andrews, St Andrews, UK
[d] Institute of Geography, University of Bern, Bern, Switzerland
[e] Alfred-Wegener-Institut Helmholtz-Zentrum für Polar- und Meeresforschung, Bremerhaven, Germany
[f] Division of Hydrological Sciences, Desert Research Institute, Reno, NV, USA

ARTICLE INFO

Keywords:
Long Island
Tarumae
Glass geochemistry
Ice cores
Sulfate
Tephra

ABSTRACT

The 17th century was a period when several major (VEI > 5) tropical and extratropical volcanic eruptions occurred. Amongst these is the VEI 6 eruption of Long Island (Papua New Guinea), which is suggested to have occurred between 1665 and 1668 CE based on historical accounts, radiocarbon dating constraints, and an ice-core record from South Pole. Accepting such an attribution on the basis of this ice-core chronology would imply a hitherto undiagnosed dating error of up to 6 years during the 17th century within all ice-core records from Antarctica. Here we constrain the timing of the Long Island eruption through tephrochronology and high-resolution glaciochemical measurements from an array of records from Antarctica and Greenland. We identify cryptotephra glass shards in association with the Greenland 1667 CE sulfate peak and geochemically attribute them to the historic Japanese Tarumae (Shikotsu) eruption. This attribution shows that the ice-core records are not misaligned during this period and refines the timing of the Long Island eruption to two candidate dates: 1654 ±1 CE and 1662 ±1 CE. Both candidate dates are within previous best age estimates based on radiocarbon dating (1651 and 1671 CE, 95.4 % probability). However, here we tentatively use 1662 ±1 CE as the timing of the Long Island eruption, as previous radiocarbon constraints suggest a 68.2 % probability of occurrence between 1655 and 1665 CE. With a higher confidence in the dating, we revised volcanic stratospheric sulfur injection (VSSI) estimates across the 17th century. Using these alongside paleo-proxy records, we explored the Northern Hemisphere climate response to the Long Island and Tarumae eruptions and found them to be more limited compared to other major (VEI >5) eruptions during this century. Ultimately, this study has highlighted the accuracy of ice core chronologies, having wider implications for volcanic forcing reconstructions and detection and attribution studies of natural climate variability.

1. Introduction

Several notable major volcanic eruptions occurred during the 17th century, including Huaynaputina (Peru) 1600 CE (White et al., 2022; Burke et al., 2023), Koma-ga-take (Japan) and Mt. Parker (Mélébingóy, Philippines) 1640 CE, and an eruption cluster with unidentified volcanic sources starting in 1694 CE (Sigl et al., 2013; D'Arrigo et al., 2020; Huhtamaa et al., 2022; Stoffel et al., 2022). Amongst the largest, with an estimated 21 km^3 airfall tephra volume and a volcanic explosivity index (VEI) of 6 (Blong and Kurbatov, 2020), is the caldera-forming eruption of Long Island, Papua New Guinea (5.33°S, 147.1°E; see Fig. 1a). Ash deposits from this eruption, referred to as the Tibito tephra, are widely dispersed across mainland Papua New Guinea (up to 400 km from the source; Coulter et al., 2009; Schneider et al., 2017). Yet, despite the large

* Corresponding authors at: Climate and Environmental Physics, Physics Institute, University of Bern, Bern, Switzerland.
E-mail addresses: imogen.gabriel@unibe.ch (I. Gabriel), michael.sigl@unibe.ch (M. Sigl).

https://doi.org/10.1016/j.jvolgeores.2025.108346
Received 31 December 2024; Received in revised form 14 April 2025; Accepted 15 April 2025
Available online 17 April 2025

magnitude of this caldera-forming eruption, and thus the potential for strong climate impacts by stratospheric sulfate injection, the precise date remains unknown due to the absence of historical records.

Determining the date of the Long Island eruption has proved challenging, with a wide range of methods employed across several disciplines, resulting in eruption ages that span three centuries (Blong et al., 2018; Blong and Kurbatov, 2020). At present, the eruption is considered to have most likely occurred in the late 17th century (1651–1671 CE, 95.4 % probability, based on radiocarbon dating and other age constraints; Blong et al., 2018). More recent efforts to further constrain the timing, based on the attribution of sulfate signals within polar ice-core records, have suggested an age of 1665–1668 CE (Blong and Kurbatov, 2020).

Polar ice cores, with their annual-layer counted chronologies, often facilitate the precise dating of past volcanic events, as they capture the atmospheric burden of sulfate aerosols and occasionally cryptotephra following a volcanic eruption (Cole-Dai, 2010; Plunkett et al., 2023). The clustering of major volcanic eruptions in the 17th century has presented challenges for some scholars in the correct attribution of volcanic sulfate layers within and between the polar ice-core records of Antarctica and Greenland. The newly proposed age of 1665–1668 CE by Blong and Kurbatov (2020) is based on their attribution of the Long Island eruption to an acidity signal in the Greenland Crete ice core peaking in 1667 CE (Hammer et al., 1980), which they link to a sulfate signal dated to 1668 CE in the Antarctic South Pole SP01 ice core (Budner and Cole-Dai, 2003). However, in other Antarctic ice-core records, this same sulfate signal is more widely dated to 1673 CE and tentatively assigned to Gamkonora (Philippines, 1673 CE; e.g., Traufetter et al., 2004; Plummer et al., 2012; Sigl et al., 2013; Nardin et al., 2020). The suggested corresponding sulfate signal in Greenland is widely assigned to the September 1667 CE Tarumae eruption in the Shikotsu volcanic system (Japan) (Sigl et al., 2013; Toohey and Sigl, 2017; Stoffel et al., 2022). This large (VEI 5) Plinian eruption of Tarumae, located in southern Hokkiado, Japan, concluded a two-millennia long period of dormancy of the volcanic system (Nakagawa et al., 2011).

Accepting the attributions of Blong and Kurbatov (2020) would indirectly imply a previously undiagnosed dating error of up to six years during the 17th century within the polar ice-core records. This would have major implications on the current forcing utilised in the Paleoclimate Modelling Intercomparison Project (PMIP)4 *past1000* simulations (Jungclaus et al., 2017) and hinder ongoing efforts to reconcile volcanic climate impact assessments in both models and proxies (e.g., Zhu et al., 2020; Fang et al., 2023). A more accurate attribution of the volcanic sulfate signals within the ice is needed to better constrain volcanic forcing during this period. This would in turn, facilitate a better assessment of the contribution of external forcing (i.e., solar radiation) to climate change, as a number of large volcanic events, including the Long Island eruption, occurred during a period of reduced solar forcing referred to as the Maunder Grand Solar Minimum (1621–1718 CE; Brehm et al., 2021, see Fig. 1b and c).

Here we re-evaluate these prior attributions and present the most likely date for the 17th century Long Island eruption. We base this on a multi-proxy investigation (combining glaciochemical records and cryptotephra analysis) on an array of polar ice-core records from both Greenland and Antarctica and consideration of radiometric and other age constraints as summarised in Blong and Kurbatov (2020). We demonstrate that the previous alignment of the South Pole (SP01, SP04) ice cores was erroneous and, when correctly aligned, the records are fully consistent with well-dated ice cores from high snow accumulation sites from across Antarctica. In addition, we present revised volcanic stratospheric sulfate injection (VSSI) estimates across the period 1590–1710 CE following this signal attribution. Using these revised forcing estimates alongside a network of proxy and climate paleoreanalysis data from across the Northern Hemisphere, we further explore the impacts of major (VEI >5) 17th century volcanic eruptions on the climate system.

2. Methods

2.1. Ice-core records

This study uses a network of ice core sulfur and sulfate records from across Greenland (NEEM-2011-S1, TUNU2013, B19, NGRIP1, EGRIP, Summit2015-composite, Summit2023, and Humboldt; McConnell, 2013; Sigl et al., 2013; Keegan et al., 2014; Sigl et al., 2015; McConnell, 2016; Sigl and McConnell, 2022; Stoffel et al., 2022; Gabriel et al., 2024; Sigl et al., 2025a) and Antarctica (WD, WDC05Q, SP01, SP04, SPC14, DML05, DML07, B40, NUS08–4, NUS08–5, NUS08–7, NUS07–2, NUS07–5, NUS07–7, DF01, DFS10, EDC96, Taylor Dome, and Talos Dome; Sigl et al., 2013; Sigl et al., 2014; Thomas et al., 2022). Together they fully cover the period 1590–1710 CE with an uncertainty across this period of ±1 year.

All Greenland ice-core records have been annual-layer counted or are volcanically synchronised to the NS1-2011 chronology (Sigl et al., 2015)

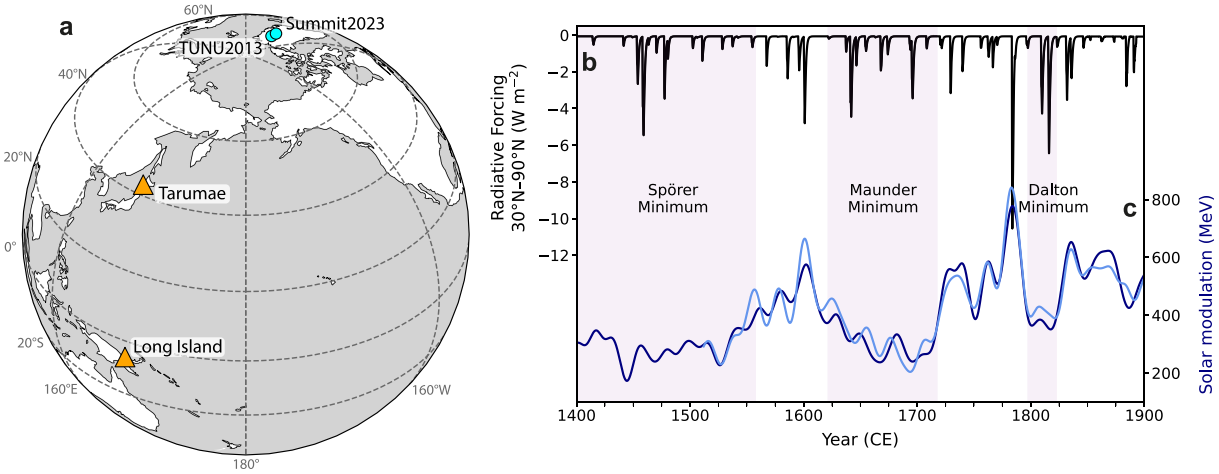

Fig. 1. **(a)** Map showing the location of the Long Island volcano (Papua New Guinea), Tarumae volcano (Japan), TUNU2013 and Summit2023 ice cores (Greenland). **(b)** Radiative forcing [30°N–90°N] (black line; Toohey and Sigl, 2017) and **(c)** Solar modulation reconstructed from ETH (navy) and QL (light blue) $\Delta^{14}C$ data (Brehm et al., 2021) between 1400 and 1900 CE. Purple shading denotes the duration of grand solar minimum events (Spörer minimum; 1388–1558 CE, Maunder minimum; 1621–1718 CE, and Dalton minimum; 1797–1823 CE). (For interpretation of the references to colour in this figure legend, the reader is referred to the web version of this article).

and all Antarctic ice-core records are consistent with the WD2014 chronology (Sigl et al., 2016), with these chronologies underpinning the latest reconstructions of volcanic forcing (Toohey and Sigl, 2017). Fluoride measurements were undertaken for the EGRIP and NGRIP1 ice cores at the Alfred Wegner Institute, Germany (AWI) and Physics of Ice, Climate and Earth, Denmark (PICE) respectively, using ion chromatography. Discrete samples at a 5 cm resolution were obtained for NGRIP1 (Siggaard-Andersen et al., 2002; Vinther et al., 2006; Plummer et al., 2012; Siggaard-Andersen et al., 2022), whilst samples for EGRIP were obtained during continuous flow analysis (CFA) measurements at the University of Bern, Switzerland using a fraction collector and have a depth resolution of ~6 cm (Schrod et al., 2020; Erhardt et al., 2023; Hörhold et al., 2025a; Hörhold et al., 2025b). Full details regarding the locations of each ice-core record used and the parameters analysed and used within this study can be found in Table A.1 and Fig. A.1.

2.2. Volcano signal detection and sulfate deposition

Sulfur deposition on the polar ice sheets is seasonally variable, non-uniform, and in the pre-industrial period consists of a background of marine-biogenic and volcanic emissions (Legrand, 1997; Cole-Dai, 2010). Following major volcanic eruptions (typically VEI >5), a volcanic excess sulfur signal is overlain on this background sulfate signal. Therefore, to isolate the volcanic signal within each ice-core record from Greenland and Antarctica and estimate the cumulative sulfate deposition (kg km^{-2}) for each volcanic eruption, we adapt previous detection methods which involve running medians of various window lengths and detection thresholds (i.e., Traufetter et al., 2004; Ferris et al., 2011; Sigl et al., 2013; see Methods A.1). We then estimate cumulative ice sheet volcanic sulfate deposition for each identified event across the study period (1590–1710 CE) by calculating mean cumulative sulfate deposition for each volcanic event across the Greenland and Antarctic ice sheets.

Owing to the highly variable accumulation rates across the Antarctic ice sheet and thus spatial variability in sulfate deposition, a weighting of 20 % was applied to the mean from all high accumulation sites and 80 % to the mean from all low accumulation sites, as adopted by Toohey and Sigl (2017). This was to derive a representative mean sulfate deposition value over Antarctica for each event. Sulfate depositional records from Greenland and Antarctica were then scaled against previous estimates used in the eVolv2k forcing reconstruction of Toohey and Sigl (2017) to provide consistency between the depositional signals and the forcing used in PMIP4 (see Fig. A.2).

In addition, to account for any smaller volcanic signals (events) which may not have been observed in the detection applied to individual records and to evaluate our threshold selection, we undertook a similar volcano detection method as discussed above, on the stacked records from Greenland (N = 7, $GRL_{1.5K}$) and Antarctica (N = 19, $ANT_{1.5K}$) (see Methods A.1). We have increased both the number and spatial coverage of records across Greenland and Antarctica compared to previous work (i.e., Sigl et al., 2013; Sigl et al., 2014; Sigl et al., 2022), thereby providing a more representative estimate of total volcanic sulfate deposition for each eruption.

2.3. Cryptotephra analysis and source attribution

A diagnostic tracer for the presence of cryptotephra in polar ice cores is an enrichment of coarse (3–10 μm), insoluble particles preceding or coinciding with concentration anomalies of volcanic volatiles (i.e, S, Cl, F) (Plunkett et al., 2023 and references therein). Measurements of insoluble particles were undertaken at the Desert Research Institute, USA using an inline Abakus® laser particle counter (Ruth et al., 2003) alongside CFA on the Greenland B19 (Gabriel et al., 2024), TUNU2013, Summit2015 (Abbott et al., 2021; Stoffel et al., 2022), and Summit2023 (this study) ice cores (see Fig. A.3). The stratigraphic co-registration of insoluble particles and sulfur peaks has proven successful in the detection of cryptotephra layers (e.g., Jensen et al., 2014; Sun et al., 2014; Dunbar et al., 2017; McConnell et al., 2020; Plunkett et al., 2020; Smith et al., 2020; Abbott et al., 2021; Plunkett et al., 2023; Abbott et al., 2024; Gabriel et al., 2024). Archived ice core sections encompassing the 1667 CE peak were subsequently sampled in the TUNU2013 ice core (from NE Greenland) between 58.04 m and 58.14 m and the Summit2023 ice core (from Central Greenland) between 108.22 m and 108.69 m for cryptotephra analysis at the University of Bern, Switzerland and University of St Andrews, UK respectively. This was to determine if glass shards were present and to use geochemical analysis to isolate their provenance.

Following the identification of glass shards within the TUNU2013_58.04m–58.14m, Summit2023_108.52m–108.69m, and Summit2023_108.22m–108.37m samples by optical microscopy, samples were prepared for electron probe microanalysis (EPMA) at the Institute of Geological Sciences, University of Bern, Switzerland and University of St Andrews, UK respectively. The full cryptotephra sample preparation method used at the University of Bern, which is adapted from several recent papers (Kuehn and Froese, 2010; Hall and Hayward, 2014; Iverson et al., 2017; Hartman et al., 2019), can be found in Gabriel et al. (2024) and that used at the University of St Andrews in Hutchison et al. (2024). In brief, both labs employed a 15 kV accelerating voltage, with a 5 μm and 2 nA beam used at the University of Bern, and a 3 μm and 1 nA beam used at the University of St Andrews. Internationally recognised secondary standards (Jochum et al., 2005; Jochum et al., 2006; Kuehn et al., 2011) were run during the analytical sessions at both labs to evaluate the precision of our measurements and facilitate robust data comparisons. All raw geochemical data (Gabriel et al., 2025a) and secondary standard data (Gabriel et al., 2025b) for analyses obtained as part of this study is publicly accessible, with full details of the operating conditions found in Table A.2.

The low abundance of cryptotephra and their small shard size (frequently <20 μm) have presented major challenges in the geochemical analysis of cryptotephra glass shards within the polar ice cores. Consequently, this has often prevented geochemical analysis of identified material and thus the attribution of volcanic fallout in ice cores to specific source eruptions. Iverson et al. (2017) suggested that a broad beam overlap method could be adopted to facilitate data acquisition where necessary, and although this method has shown a decrease in precision (i.e., lower analytical totals), all the elements have been shown to be statistically similar. The adoption of this approach has resulted in confident geochemical attributions in other cryptotephra studies (i.e., Dunbar et al., 2017; Abbott et al., 2024; Innes et al., 2024) and was therefore adopted within this study on the TUNU2013 samples, where shards were small (≤20 μm) and low in abundance (N = ≤10). We filtered the data to totals >75 wt. %, with a lower total threshold selected to account for this small shard size (<20 μm) and the subsequent overlap with the epoxy resin. In both Summit2023 samples, glass shards were more abundant (N = ≥20), increasing the chance of a more confident geochemical analysis and thus a higher total filter threshold of >90 wt. % was used.

To facilitate correlations to existing published datasets, P_2O_5 and Cl were removed from our obtained data to ensure secure comparisons. Data was then normalised to an anhydrous basis following standardised practices. Following normalisation, the data from the TUNU2013_58.04m–58.14m and Summit2023_108.52m–108.69m samples formed a single homogenous population, despite the differences in the raw total oxide values. The data were correlated to compiled published tephra geochemical data for candidate eruptions consisting of both proximal and distal deposits, with these correlations explored graphically.

2.4. Estimating stratospheric sulfur injection

Estimates of stratospheric sulfur injection following a volcanic eruption require the cumulative sulfate deposition from the ice sheets

for each volcanic event, along with the latitude and timing of the injection, to be known. For many of the eruptions across the study period 1590–1710 CE, the latitude and timing was assigned using historical records and global inventories of volcanism (i.e., Global Volcanism Program (Global Volcanism Program, 2024)). However, where the volcanic signal within the ice-core records was unattributed and thus the latitude was unknown, a default latitude of 0° was used for unidentified events with a bi-polar signal (i.e., a tropical eruption) and 45°N and 45°S for unidentified extratropical eruptions in the Northern and Southern Hemispheres respectively, following Toohey and Sigl (2017).

The full method for estimating volcanic stratospheric sulfur injection (VSSI) is described in detail by Toohey and Sigl (2017) and Sigl et al. (2022) and is based on the assumption that the sulfur deposition recorded in the ice cores is proportional to the stratospheric sulfur injection. Briefly, mean ice sheet cumulative sulfate deposition for Greenland (f_G) and Antarctica (f_A) are related to injected sulfur mass (M_S) in Eq. (1):

$$M_S = \frac{1}{3}\left[L_G f_G + L_A f_A\right] \quad (1)$$

L_G and L_A are transfer functions which account for the spatial distribution of sulfate deposition over each hemisphere, which has been based on the analysis of the spread and deposition of nuclear bomb test fallout, sulfate from well-studied historic volcanic eruptions (i.e., Pinatubo 1991 CE), and the analysis of atmospheric aerosol model experiments. Following previous work (Gao et al., 2007; Gao et al., 2008; Crowley and Unterman, 2013; Toohey and Sigl, 2017; Sigl et al., 2022), we apply transfer function estimates of 1×10^9 km^2 for tropical eruptions, 0.57×10^9 km^2 for extratropical eruptions, and 0.1×10^9 km^2 for Icelandic eruptions (see Table 1). For Northern Hemisphere extratropical eruptions, revised (0.44×10^9 km^2) estimates of the transfer function and larger uncertainties have recently been proposed (Fuglestvedt et al., 2024). We report these in addition to the other reported values for consistency with existing reconstructions of volcanic forcing in Table A.3.

2.5. Estimating the latitude and timing

Monthly resolved non-sea-salt (nss) sulfur (Sigl et al., 2025b) and insoluble particle records from the Summit2015-composite (Greenland) and a nss-S record from WDC (Antarctica) were used to help constrain the timing of the largest volcanic and partly overlapping sulfate depositional signals, which we attributed to concurrent volcanic eruptions within a few months to years of each other. Using these highly resolved records, it was possible to separate the volcanic events by approximating

Table 1
Summary of revised volcanic stratospheric sulfate injection (VSSI) estimates across the period 1590–1710 CE. Volcano name, eruption start date [CE], latitude [°N] (if known – otherwise default latitudes based on Toohey and Sigl (2017) are used), cumulative event volcanic SO_4 [kg km^{-2}] deposition for Greenland and Antarctica, and VSSI [Tg S] with 1σ uncertainty provided in brackets. VSSI estimates are shown for this study, alongside previous estimates from Toohey and Sigl (2017) used in PMIP4. Bold text indicates the VSSI estimates for the five sulfate peaks identified within the ice-core records which have subsequently been divided based on the monthly sulfur records.

Volcano		Eruption Date [CE]	Latitude [°N]	VolSO$_4$ (kg km^{-2})		VSSI (Tg S) [± 1σ uncertainty]	
				Greenland flux	Antarctic flux	This study	PMIP4 [a]
Fuijisan (Japan)	–	December 1707	35.4	13	*N/A*	2.5 [0.7]	1.1 [0.4]
Unidentified		**1694**	**0**	**31.1**	**22.1**	**17.7 [2.6]**	**15.7 [2.9]**
	UE 1697	1697	-45	*N/A*	3.5	0.7 [0.2]	–
	UE 1696	1696	0	7.8	2.9	3.5 [1.0]	–
	UE 1695	1695	0	8.7	9.5	6.1 [1.5]	–
	UE 1694	1694	0	14.6	6.2	6.9 [2.0]	–
Gamkonora (Indonesia)	–	May 1673	1.38	6.5	8.1	4.6 [0.7]	4.7 [0.8]
Tarumae (Japan)		**September 1667**	**42.69**	**21**	***N/A***	**4.9 [1.0]**	**3.5 [1.1]**
	UE 1669	1669	45	1.7	*N/A*	0.3 [0.1]	–
	Tarumae (Japan)	September 1667	42.69	19.4	*N/A*	3.7 [1.4]	3.5 [1.1]
Long Island (Papua New Guinea)	–	1662	-5.36	8.3	4.4	4.2 [0.8]	0.8 [0.1]
Unidentified	–	1654	0	7.5	6.5	4.7 [1.0]	3.7 [1.2]
Unidentified	–	1645	45	15	*N/A*	2.8 [0.9]	2.4 [0.8]
Mt. Parker [Mélébingóy] (Philippines)		**26th December 1640**	**6.11**	**45.6**	**14.4**	**20.0 [3.3]**	**18.7 [4.3]**
	Mt. Parker [Mélébingóy] (Philippines)	26th December 1640	6.11	37.4	14.4	17.3 [4.6]	–
	Koma-ga-take (Japan)	July–October 1640	42.06	8.2	*N/A*	1.6 [0.6]	–
Hekla (Iceland)	–	February 1636	63.98	13.5	*N/A*	0.5 [0.1]	1.3 [0.5]
Unidentified	–	1625	45	12.5	*N/A*	2.4 [0.8]	1.6 [0.3]
Unidentified	–	1622	-45	*N/A*	8.4	1.6 [0.2]	–
Huaynaputina (Peru)		**19th February 1600**	**-16.61**	**28.7**	**18.3**	**15.7 [2.6]**	**18.9 [4.0]**
	Huaynaputina (Peru)	19th February 1600	-16.61	23.8	18.3	14.0[3.2]	–
	Paektu (China/DPRK)	1600	41.98	4.9	*N/A*	0.9 [0.4]	–
Nevado del Ruiz (Colombia)		**1595**	**-4.89**	**15.8**	**14.9**	**10.3 [1.8]**	**8.9 [1.5]**
	Unidentified	1596	0	9	6.1	5.1 [1.5]	–
	Nevado del Ruiz (Colombia)	1594	-4.89	6.8	8.8	5.2 [1.4]	–
Unidentified	–	1590	-45	*N/A*	6.8	1.3 [0.4]	0.5 [0.3]

N/A indicates no sulfur deposition on ice sheet for that event.
[a] Based on Toohey and Sigl (2017).

the start and end date of each sulfur peak. This in turn allowed the total deposited volcanic sulfate across the peak to be redistributed amongst these individual eruptions within the ice-core records (see Figs. A.4, A.5, and A.6). To incorporate these within our VSSI estimate, a 30 % uncertainty was assumed in peak separation.

For the smallest volcanic sulfur signals, such as 1662 CE, it remains challenging to precisely quantify the start and duration of these events. This in on account of the small size of the volcanic sulfur signal relative to the natural sulfur cycle, and the large variability of these small signals across all ice-core records. However, through improved detection methods and increasing the number and spatial coverage of highly-resolved ice-core records, we have been able to provide more representative estimate of total volcanic sulfate deposition for these smaller eruptions (see Section 2.2).

2.6. Temperature reconstructions and climate impact assessment

We explore the Northern Hemisphere temperature response to the 1662 CE (which we tentatively assign to Long Island) and Tarumae 1667 CE eruptions compared to the four largest eruptions (1595 CE Nevado del Ruiz, 1600 CE Huaynaputina, 1640 CE Mt. Parker, and the 1694 CE unidentified eruption cluster), across the study period using a combination of stable water isotope ($\delta^{18}O$) records from Greenland, summer temperature proxy data (Wilson et al., 2016), and climate paleo-reanalysis data, which combines such proxy records with model simulations, early instrumental data, and documentary sources (Valler et al., 2023; Valler et al., 2024).

We collate 15 high-resolution published $\delta^{18}O$ records from sites across the Greenland ice sheet (GRIP, NGRIP1, EGRIP, Summit2015-composite, NEEM-2011-S1, B17, B18, B21, B23, B26, B27/B28, B29, B30, GISP2, and Crete; Weißbach et al., 2016; Osman et al., 2021; Hörhold et al., 2023; Rasmussen et al., 2023). These records were selected as each record (1) covers the period 1590–1710 CE, (2) has at least an annual resolution, (3) and has a high age accuracy. We compile the dataset of 15 $\delta^{18}O$ records into a single stack by calculating the mean $\delta^{18}O$ value for each year. A conversion from isotopic composition to temperature (°C) was estimated through linear regression with a calibration slope of 0.77°C/ ‰, calculated using paleo-reanalysis data from a spatial grid over Greenland between 1800 and 1980 CE (Fig. A.7). The uncertainty for our temperature reconstruction was estimated to be 0.4°C and was calculated using the root mean square error (RMSE) across the verification period (1699–1799 CE; Fig. A.7). In addition, we compare our results to a range of other independent calibration slopes derived for ice cores from Greenland (Hörhold et al., 2023 and references therein). Annual temperature anomalies (°C) were calculated with respect to the 1550–1750 CE interval (Fig. A.8) to isolate a post-volcanic cooling response to these volcanic eruptions. Further details on the calibration method can be found in Methods A.2.

The Northern Hemisphere temperature response to selected eruptions was additionally explored through spatial composite analysis using the Modern Era Re-analysis (ModE-RA) global climate reanalysis data (Valler et al., 2023). ModE-RA is a global paleo-reanalysis covering the period 1422–2008 CE, reconstructing the past climate through the assimilation of natural proxies, documentary, and instrumental measurements into a climate model simulation ensemble (Valler et al., 2024). Annual temperature anomalies with respect to 1550–1750 CE were used, and composite maps were constructed for four periods (DJF, MAM, JJA, and SON) in the year of and up until three years after the eruption.

We use Superposed Epoch Analysis (SEA; Haurwitz and Brier, 1981) to explore the mean temporal temperature response across the Northern Hemisphere to the selected eruptions using our Greenland $\delta^{18}O$ stack (N = 15), ModE-RA global climate paleo-reanalysis data, and N-TREND tree-ring data. The latter is a tree-ring based summer (MJJA) temperature reconstruction encompassing 54 records from across the Northern Hemisphere covering the period 918 to 2004 CE (Wilson et al., 2016; Anchukaitis et al., 2017). To facilitate this analysis, temperature anomalies were calculated for each dataset with respect to a five-year period void of any known volcanic eruptions closest to each volcanic event (Table A.4). The start years of these selected eruptions were validated with historical records. SEA was restricted to five years after each event due to the strong clustering of many events. The statistical significance of any post-eruption cooling response was calculated using a Mann-Whitney *U* test.

3. Results and discussion

3.1. Signal attribution and the timing of the Long Island eruption

The recently proposed age for the 17th century eruption of Long Island, based on ice-core records from South Pole, is 1665–1668 CE (Blong and Kurbatov, 2020). Across this proposed age span in ice cores from Greenland, a large increase in sulfur concentrations in 1667 CE is observed (Fig. 2). This signal, which is absent from Antarctica (see Fig. 2), is widely attributed to the eruption of Tarumae (Shikotsu), Japan. A sharp peak in insoluble particles (2.6–10 μm; Figs. A.3 and A.4) coincides with the rise of the sulfur peak beginning in 1667 CE in the Greenland B19, Summit2015, Summit2023, and TUNU2013 ice cores. A smaller separate sulfur peak only present in the Greenland Summit2015, NEEM-2011-S1, and Summit2023 ice cores is observed in 1669 CE, and was also accompanied by a smaller particle peak (Fig. A.4). Both peaks were sampled for cryptotephra geochemical analysis in Summit2023 (Fig. A.4), and the 1667 CE peak was sampled in TUNU2013 (Fig. 2a). Glass shards identified in the TUNU2013 (N = ≤10) and Summit2023 (N = ≥30) 1667 CE samples were colourless with mostly thin platy-cuspate morphologies and a diameter of 10–25 μm in size (see Fig. A.9). In the Summit2023 1669 CE sample a total of 18 glass shards were identified. Fifteen of these had a slightly larger size (a diameter of 15–40 μm) and were colourless-yellow with platy – angular morphologies, whilst 3 shards had a diameter of 15–20 μm and very vesiculated rounded edges.

Major element geochemical data obtained from these glass shards was plotted alongside geochemical fields for the Shiveluch (SH-1) 1652 ±11 CE, Long Island (Tibito), and Tarumae (Ta-b) eruptions, as the age uncertainties of all three events fall within the proposed age range. Major element geochemical analysis of the identified glass shards from the TUNU2013 and 1667 CE Summit2023 samples provides a correlation with the VEI 5 Tarumae eruption (Ta-b tephra) (see Fig. 3) and are geochemically distinct from that of the Long Island eruption fallout. Next to eruptions of Towada (To-H; Cook et al., 2022) and Mashu (Davies et al., 2024) this is the third eruption from Japan identified in the Greenland ice cores. Geochemical analysis of the Summit2023 1669 CE sample yields two geochemically distinct populations; group 1, a trachyandesite population (comprising 15 shards) and group 2, a trachydacite population (comprising only of 3 shards, Fig. 3). These analyses do not provide a correlation with any of the known events during this period, as identified in global inventories of volcanic eruptions (i.e., Global Volcanism Program; Global Volcanism Program, 2024).

The attribution of the Greenland 1667 CE ice core volcanic sulfate signal to Tarumae shifts the search window for the 17th century eruption of Long Island to other candidate events in the 1650s and 1660s and extends the known dispersal range of the Ta-b tephra to northeastern Greenland (>6000 km from source). Additionally, our attribution of the 1667 CE volcanic signal in Greenland highlights that previous attributions from the South Pole Antarctic ice cores (SP04 and SP01) are erroneous, which implies these ice-core records are misaligned (Budner and Cole-Dai, 2003; Ferris et al., 2011). A dating bias has previously been detected in the SP04 ice core (~ 150-years around 434 CE; Sigl et al., 2014) and has mostly been attributed to the site's low accumulation rate (<8 cm yr^{-1}) and local glaciological surface processes (Ferris et al., 2011). Owing to this, Sigl et al. (2014) corrected the dating of these records, amongst others, through precise synchronisation to the

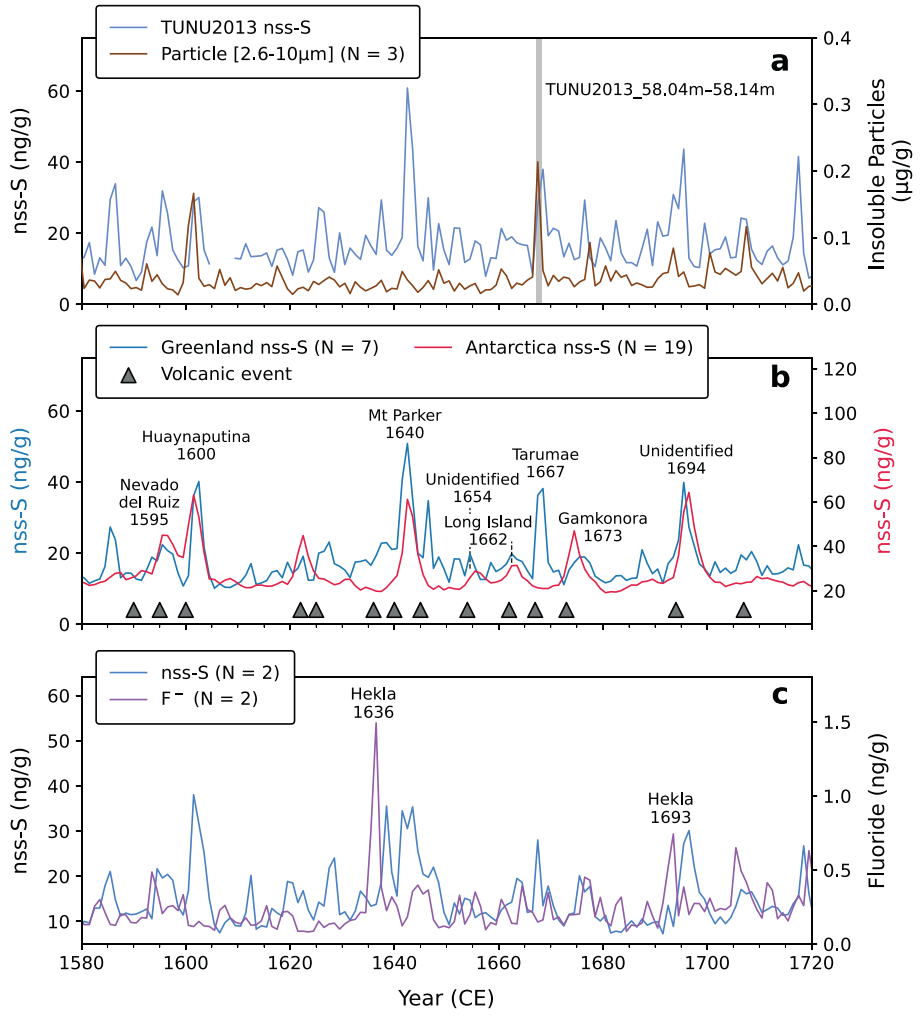

Fig. 2. Ice core volcanic tracers across the 17th century. **(a)** TUNU2013 non-sea-salt sulfur (nss-S) record and Greenland insoluble particle records (N = 3). Grey shading denotes cryptotephra sampling window of the particle peak associated with the 1667 CE volcanic sulfur signal. **(b)** Greenland nss-S record (N = 7) and Antarctica nss-S (N = 19). 14 volcanic events (grey triangles) were identified across our study period (1590–1710 CE), representing 21 volcanic eruptions. Events discussed in detail are labelled. **(c)** NGRIP1 and EGRIP nss-S and fluoride (F^-) records. Enrichments are observed at the time of the historic Icelandic Hekla 1636 CE and 1693 CE eruptions.

WD2014 chronology (Sigl et al., 2016) (Fig. A.10). The WD2014 chronology provides improved dating accuracy due to the higher accumulation rates and consistent annual layering at the WDC site. As a result, it has been used in the development of the SPC19 chronology for the SPC14 ice core which contains a volcanic signal in 1662 CE (Winski et al., 2019). Utilisation of this highly resolved record shifts the SP01 and SP04 Antarctic 1668 CE peak to 1662 CE, consistent with other Antarctic records. We therefore suspect that in the search for Long Island, Blong and Kurbatov (2020) used the original dating based on annual-layer counting of the South Pole (SP01) ice core (Budner and Cole-Dai, 2003). This was only later synchronised to the precise WDC chronology (Sigl et al., 2014), thereby resulting in a misinterpretation of the volcanic signals in the mid-17th century.

Using our stack of annually resolved Greenland and Antarctic sulfur records, which have a dating uncertainty of ±1 year across the study period, we identify the 1662 CE and 1654 CE signals as the only unattributed bi-polar peaks within the 2-sigma search window for the Long Island eruption suggested by Blong et al. (2018) (Fig. 2b). The moderate 1662 CE sulfur peak has previously been identified in the Antarctic records (Sigl et al., 2014), but not in Greenland, and we consider this to be the most likely candidate for the 17th century eruption of Long Island, owing to previous radiocarbon constrained best age estimates (1655–1665 CE; 68.2 % probability (Blong et al., 2018)). Through our identification of a smaller sulfate peak with an unidentified source in 1669 CE, we have redistributed the ice core deposited volcanic sulfate for the Tarumae 1667 CE eruption using the monthly resolved Summit data, with Tarumae accounting for 92 % of the deposited volcanic sulfate (Fig. A.4).

In total, we identify 14 volcanic events in our stacked ice-core records across the period 1590–1710 CE (Fig. 2b), representing 21 different eruptions (Table 1). The detected eruption frequency is 0.16 yr^{-1} which is 40 % larger than the estimated mean eruption frequency for the past 2500 years (Toohey and Sigl, 2017) and 50 % larger compared to the Holocene (Sigl et al., 2022). The increased eruption frequency in the 17th century compared to the long-term mean is the result of higher volcanic activity at this time, next to an improved ability to detect and resolve smaller eruptions using the comprehensive network of ice cores in this study and the availability of more ice cores covering this time period.

3.2. *Attribution and timing of other 17th century volcanic eruptions*

Absent from our stack of Greenland sulfur records (Fig. 2b) is the 1693 CE February eruption of Hekla, Iceland, the timing of which is confirmed through historical sources and geological records (Thordarson and Larsen, 2007; Janebo et al., 2016; Pedersen et al.,

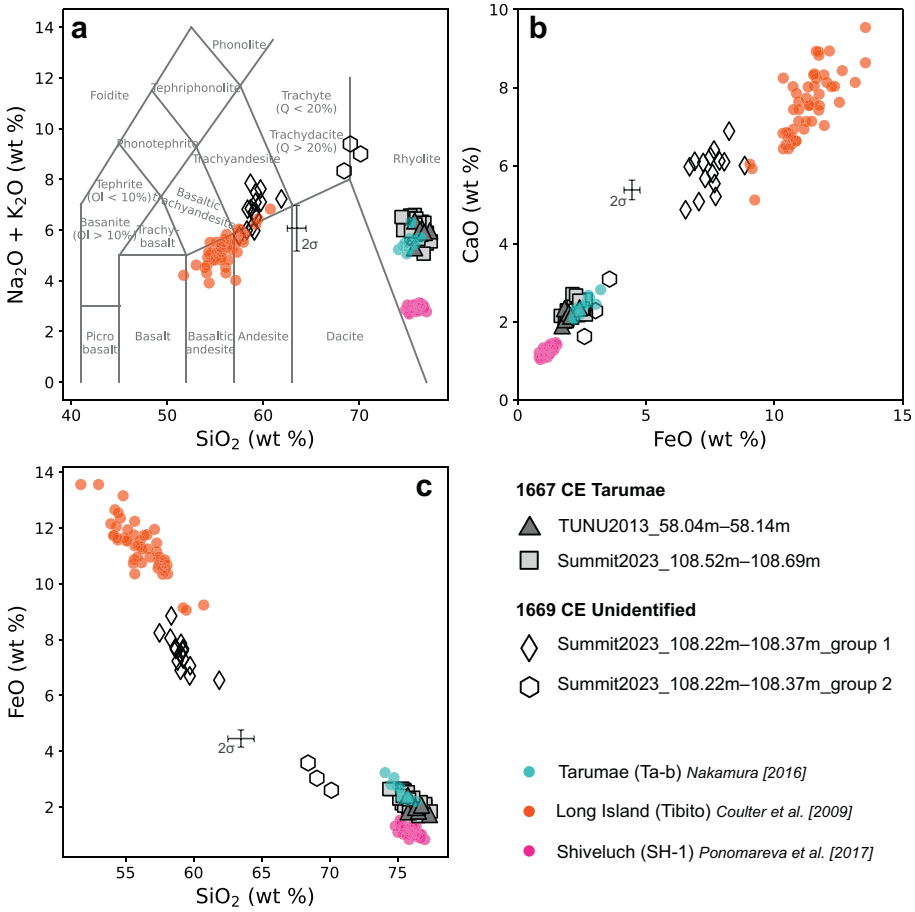

Fig. 3. Major element geochemical data from individual glass shard analyses from cryptotephra horizons in the Greenland TUNU2013 and Summit2023 ice cores. Data has been plotted based on **(a)** magmatic composition – Total Alkali ($Na_2O + K_2O$) vs Silica (SiO_2) (Le Maitre et al., 2002); **(b)** FeO vs CaO; and **(c)** SiO_2 vs FeO. Ice core sample analyses from TUNU2013 (triangle) and Summit2023 (square) which have been geochemically attributed to the Tarumae (Japan) 1667 CE eruption are shown. Two (group 1 (diamond) and group 2 (hexagon)) additional geochemically distinct populations from the Summit2023 1669 CE sample with unidentified sources are also shown. All ice core data are plotted alongside published geochemical analyses associated with the Tarumae Ta-b tephra (blue dots; Nakamura, 2016), Long Island Tibito tephra (orange dots; Coulter et al., 2009), and Shiveluch SH-1 tephra (pink dots; Ponomareva et al., 2017). Error bars represent 2 standard deviations (2σ) of repeat analysis of the StHs6/80-G secondary standard. All data have been normalised to 100 wt. % (anhydrous basis). (For interpretation of the references to colour in this figure legend, the reader is referred to the web version of this article).

2018). A broad sulfur peak, beginning in 1694 CE and lasting until 1700 CE in some ice cores, is observed in both Greenland and Antarctic records and has previously been attributed to an event with an assumed tropical source. Monthly sulfur data from the Greenland Summit2015 ice core does, however, show a small sharp single separate peak in 1693 CE (21.3 ng/g) coinciding with a pronounced peak in insoluble particles (Fig. A.5d). The detection of smaller volcanic events and the separation of clustered volcanic events is possible in Summit2015, due to the high accumulation rate (22 cm yr^{-1}; Maselli et al., 2017) at the drill site.

Coinciding with this single sulfur peak in 1693 CE is a pronounced enrichment (0.73 ng/g) in a stacked fluoride record from the NGRIP1 and EGRIP ice cores, with a more prominent peak in fluoride observed at the time of the larger 1636 CE Hekla eruption (1.49 ng/g) (Fig. 2c). Observations of past Hekla eruptions (i.e., 1947, 2000) have shown that this volcanic system is characterised by enrichments in fluorine (Sigvaldason and Óskarsson, 1986; Moune et al., 2006). Previous studies have suggested the use of volcanic volatiles and heavy metals as an indicator for volcanic activity more proximal to ice core sites (Mason et al., 2022; Gabriel et al., 2024; McConnell et al., 2024), due to the behaviour of such volcanic volatiles (i.e., rapid scavenging from the plume with increased distance; Ilyinskaya et al., 2021). Proximal isopach mapping confirms a general northwest direction of the Hekla 1693 CE eruption plume towards Greenland (Janebo et al., 2016). Following this and based on the attribution of other Icelandic volcanic eruptions due to enrichments in these species within the Greenland ice-core records, we attribute the 1636 CE and 1693 CE fluoride peaks to the Hekla eruptions of the respective years. This latitudinal assignment has allowed improvements to be made in pre-existing forcing reconstructions used in eVolv2k (Toohey and Sigl, 2017).

In addition, using the monthly resolved Summit2015 and WDC sulfur records, we identify four volcanic sulfur peaks across the period 1694–1700 CE, which we attribute to one Southern Hemisphere extratropical eruption and three tropical eruptions (Figs. A.5d and A.6d). Global inventories of volcanism (i.e., Global Volcanism Program; Global Volcanism Program, 2024) suggest that during the 1690s CE several large eruptions occurred, including eruptions from Indonesia and Japan. However, with cryptotephra yet to be identified across this period in the polar ice-core records, no confident attributions have been made. Therefore, we refer to this broad sulfate peak as the unidentified 1694 CE event but acknowledge that this depositional signal could be the result of a cluster of eruptions.

Our monthly resolved glaciochemical dataset further allowed separation and the distribution of ice core deposited volcanic sulfate for the 1595 CE event (Figs. A.5a and A.6a), the 1640 CE double event of Mt. Parker and Koma-ga-take (Figs. A.5b and A.6b), and the 1600 CE Huaynaputina eruption from a presumed Northern Hemisphere extratropical source (Figs. A.5c and A.6c). The latter has been previously identified during recent S isotope analyses (Burke et al., 2023) and

tentatively assigned to Paektu (China, DPRK; Plunkett et al., 2023).

Having constrained the timing and source of volcanic signals across the period 1590–1710 CE, we present revised estimates of volcanic stratospheric sulfur injections (VSSI) for the 17th century (see Table 1). These are based on new arrays of ice cores from across Greenland and Antarctica (Fig. A.1), increasing the number of records used in current estimates for Greenland and Antarctica from three and 14, to seven and 19 respectively. VSSI estimates do not change significantly across the period, with Mt. Parker (Mélébingóy) (17 ±5 Tg S), Huaynaputina (14 ±3 Tg, S), the unidentified 1694 CE event (7 ±2 Tg S), and Nevado del Ruiz (5 ±2 Tg S), remaining as the four largest events of 1590–1710 CE, despite the small, applied reductions resulting from the separation of contemporaneous volcanic eruptions. Using these revised estimates, we have explored the climate impacts following these eruptions across the Northern Hemisphere where there is an extensive network of paleo-environmental and historical proxy records.

3.3. Northern Hemisphere climate impacts of 17th century volcanic eruptions

The climatic impacts following the major eruptions across the study period, i.e., Huaynaputina 1600 CE and Mt. Parker 1640 CE, have been the subject of several studies, with strong cooling and long-lasting socio-economic impacts experienced following these events (i.e., De Silva and Zielinski, 1998; Fei et al., 2016; Huhtamaa and Helama, 2017; Stoffel et al., 2022; White et al., 2022). Our Greenland $\delta^{18}O$ stack (N = 15) shows pronounced regional cooling anomalies following the Huaynaputina 1600 CE and Mt. Parker 1640 CE eruptions (−0.6°C), as well as the third and fourth largest VSSIs of the period, the unidentified event in 1694 CE (−0.8°C) and Nevado del Ruiz in 1595 CE (−0.5°C) (Fig. 4a). Superposed epoch analysis (SEA) of temperature reconstructions (tree-rings, Greenland $\delta^{18}O$ records, and paleo-reanalysis data) show that this post-volcanic cooling is most pronounced one to two years after the eruptions (Fig. 4b).

In agreement with previous studies, our composite map analysis suggests that cold summers (JJA) [with respect to 1550–1750 CE] were experienced across the Northern Hemisphere following the 1600 CE Huaynaputina and 1640 CE Mt. Parker eruptions (Fig. 5b and c, Figs. A.11 and A.12). However, Burke et al. (2023) suggested that some of the cooling following Huaynaputina 1600 CE could be attributed to a Northern Hemisphere extra-tropical eruption which coincided with Huaynaputina in 1600 CE, tentatively linked to Paektu (China, DPRK) based on a single tephra shard (Plunkett et al., 2023). Both the 1595 CE eruption of Nevado del Ruiz and the unidentified 1694 CE event show a

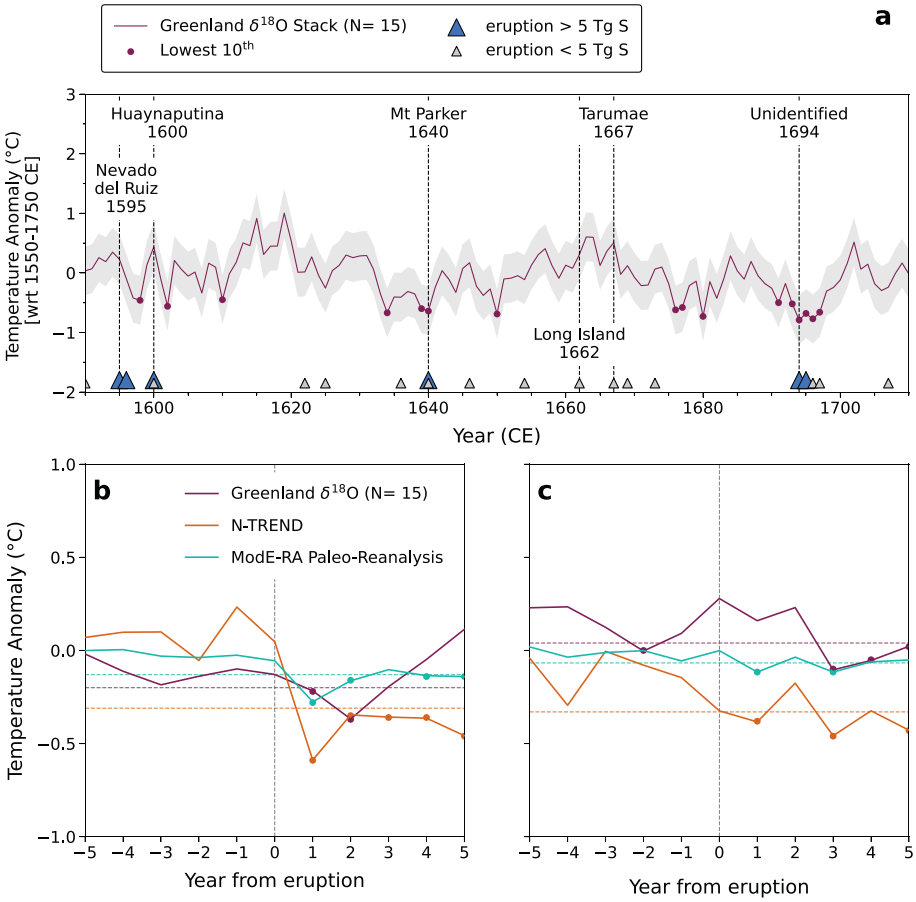

Fig. 4. **(a)** Greenland $\delta^{18}O$ (N = 15) annual temperature anomaly (°C) with respect to 1550–1750 CE (purple line). Purple circles denote years in the lowest 10th percentile of the entire stable isotope stacked record (1400–2011 CE). Grey shading shows the calculated 0.4°C uncertainty in our reconstruction. Eruptions with an estimated VSSI >5 Tg S are shown by blue triangles and those with <5 Tg S by grey triangles. Volcanic eruptions for which the climate impacts have been explored within this study are marked. **(b)** Mean Northern Hemisphere climate response to the four largest VSSIs across the study period 1590–1710 CE in annual mean Greenland $\delta^{18}O$ (N = 15; this study), boreal summer N-TREND (Wilson et al., 2016), and annual mean ModE-RA climate paleo-reanalysis datasets (Valler et al., 2023). **(c)** Mean Northern Hemisphere temperature response to the 1662 CE Long Island and 1667 CE Tarumae eruptions in annual mean Greenland $\delta^{18}O$ (N = 15; this study), boreal summer N-TREND, and annual mean ModE-RA climate paleo-reanalysis datasets. 5 years prior and 5 years after the eruption year (Year 0) are shown. Horizontal dashed lines show *p*-value (<0.05) for annual mean Greenland $\delta^{18}O$ (N = 15; purple), boreal summer N-TREND (orange), and annual mean ModE-RA climate paleo-reanalysis (blue) calculated using the Mann-Whitney *U* test. Circles mark years which fall below this threshold and thus are considered statistically significant. (For interpretation of the references to colour in this figure legend, the reader is referred to the web version of this article).

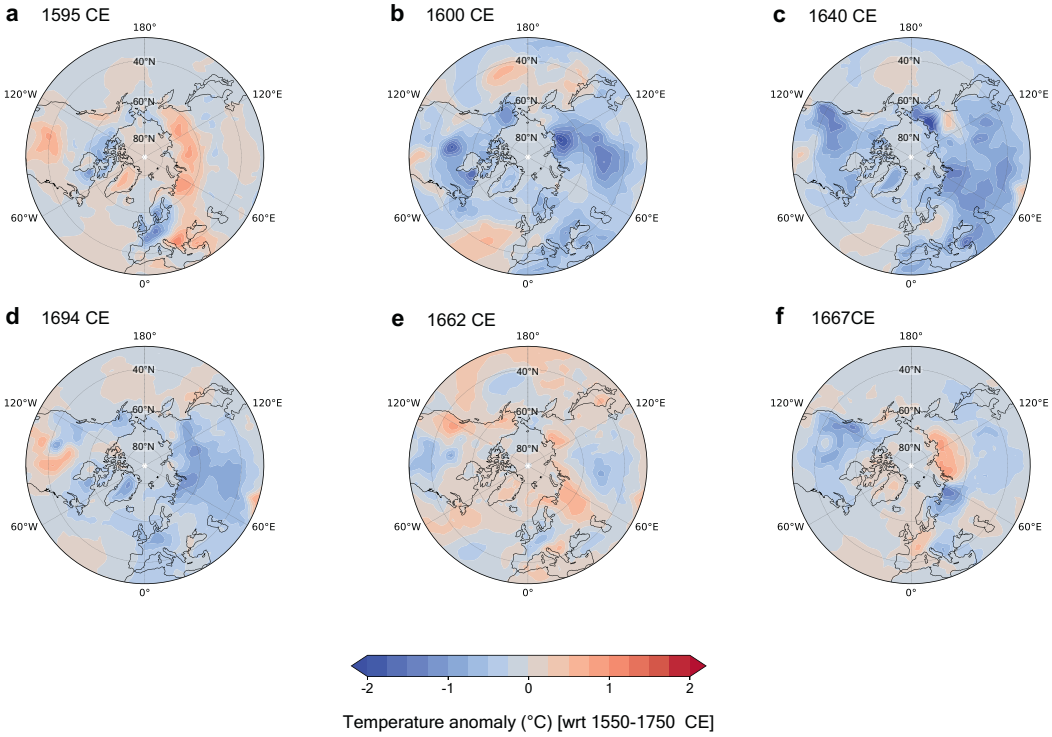

Fig. 5. Summer (June–August) temperature anomaly (°C) [30°N–90°N] in the years of and 3 years after the volcanic eruptions of **(a)** Nevado del Ruiz, 1595 CE, (b) Huaynaputina, 1600 CE, **(c)** Mt. Parker [Mélébingóy], 1640 CE, **(d)** the unidentified event, 1694 CE, **(e)** Long Island, 1662 CE, and **(f)** Tarumae, 1667 CE using ModE-RA (Valler et al., 2024). Data visualisation is based on ClimeApp (Warren et al., 2024). Anomalies are calculated with respect to 1550–1750 CE.

similar summer cooling signature. Whilst a considerable amount of the cooling following the unidentified 1694 CE event occurred in Europe and Asia, much of the cooling that followed the 1595 CE Nevado del Ruiz eruption was confined to Central and Northern Europe (Fig. 5a and d; Figs. A.13 and A.14).

Notably, the Greenland $\delta^{18}O$ records show that several of the coldest years (6 of the 69 lowest 10th percentile) of the entire compiled stable isotope record (1400–2011 CE) occurred at the time of and after the unidentified 1694 CE event (Fig. 4a), with the 1690s CE considered amongst the coldest periods of the Little Ice Age within Europe (Wanner et al., 2022). Finnish historical records cite that impacts on harvests already began in 1693 CE and conditions were exacerbated by successive severe winters, most notably in 1694–1695 CE, with the latter coinciding with a strong negative North Atlantic Oscillation (NAO) (Luterbacher et al., 1999; Luterbacher et al., 2001; Huhtamaa et al., 2022). This prolonged and pronounced cooling could therefore be a consequence of both natural variability (i.e., a negative NAO and low solar activity) and the clustering of three tropical volcanic eruptions, which we have attributed to the broad 1694 CE sulfur peak.

In contrast, both the 1662 CE eruption (which we tentatively link to Long Island) and the 1667 CE eruption (confirmed as Tarumae) appear to have caused limited post-volcanic cooling in the Northern Hemisphere (Fig. 5e and f), with a variable response detected in the SEA of Greenland ice-core records, tree-ring, and paleo-reanalysis datasets (Fig. 4c). An absence of a cooling signature in the Greenland records may be due to the winter warming, beginning in the early 1660s CE, occurring over Greenland and the Arctic (Figs. A.15 and A.16). Several studies have shown that background conditions play an important role in determining the response of the climate system to a volcanic eruption (Zanchettin et al., 2013; Weierbach et al., 2023). However, these studies have only focused on strong (i.e., Pinatubo–Tambora sized) tropical volcanic eruptions. Thus, the response to much smaller VSSIs (≤5 Tg S) would need to be further explored via climate model simulations, as the quantity of sulfur injected into the stratosphere is a key parameter dictating the climate response (Toohey and Sigl, 2017; Marshall et al., 2019; Marshall et al., 2020; Sigl et al., 2022).

The low VSSI of the Long Island eruption (4 ±1 Tg S) is a likely explanation for its negligible climate impacts within the Northern Hemisphere. Although the caldera-forming eruption of Long Island was ash-rich (airfall tephra volume >21 km^3; Blong and Kurbatov, 2020), having an estimated explosivity comparable to the 1883 CE eruption of Krakatau (bulk volume >16 km^3; Self, 1992), the ice-core records suggest that it was sulfur poor, with an estimated VSSI of 4 Tg S compared to the 9 Tg S of Krakatau (Toohey and Sigl, 2017). This is similar to other eruptions with large magnitudes but limited atmospheric sulfur injections (i.e., Santorini, Taupō, Paektu Millennium Eruption; Pearson et al., 2022; Piva et al., 2023; Scaillet and Oppenheimer, 2024; Lee et al., 2024) and reiterates that a large erupted tephra mass does not necessarily equate with a higher atmospheric sulfur loading and thus stronger climate impacts. However, the large volume of erupted material did have significant local impacts; reshaping the island and its vegetation and affecting nearby communities on mainland Papua New Guinea (Blong, 1982; Thornton et al., 2001).

The limited climate impacts following the 1667 CE Tarumae eruption could be explained by a greater burden of the sulfate aerosols being retained and transported in the troposphere towards the Greenland ice sheet. Unlike tropical eruptions, a large proportion of the sulfur ejected from extratropical eruptions does not have to be injected into the stratosphere for the volcanic signal to be detected in the polar ice sheets (i.e., Burke et al., 2019). In the troposphere, injected sulfur has a shorter residence time (days to weeks) than sulfur which reaches the stratosphere (months to years) and thus, the climate impacts associated with tropospheric eruptions are typically less pronounced (Robock, 2000; Cole-Dai, 2010). Ultimately, S isotope analysis (Burke et al., 2019; Burke et al., 2023) of sulfate preserved within the Greenland ice cores associated with the Tarumae eruption may offer further insights. This method allows the discrimination between sulfate that reached the stratosphere and that which remained in the lowermost stratosphere/

troposphere and has been applied to the 1600 CE eruption of Huaynaputina, quantifying the stratospheric burden of sulfate for this eruption (Burke et al., 2023). However, as with the eruption of Long Island, the localised impacts following the Tarumae eruption were far more pronounced, with Hokkaido's vegetation impacted by pyroclastic flows and ash fall deposits (Oka and Takaoka, 1996; Namikawa et al., 1997).

3.4. Spatial and seasonal biases in temperature reconstructions

Climate reconstructions for these eruptions are invariably biased to Northern Hemisphere records, despite five of the six eruptions being tropical eruptions. This is due to the scarcity of available proxies within the Southern Hemisphere, with the PAGES2k database for example (PAGES2k Consortium, 2017), having few (<16 % of all archives) high-resolution records from the Southern Hemisphere (e.g., Neukom et al., 2014). If such records were available, a better assessment of the global impacts of the caldera forming Long Island eruption, here tentatively dated to 1662 ±1 CE, would be possible, with a stronger response potentially observed in Southern Hemisphere proxies.

Moreover, most volcano-climate impact studies have focused on the summer temperature response to volcanic eruptions, which we have also largely done in this study. This is on account of many of the existing records (i.e., tree-rings) having a strong seasonal bias. However, it is well known that the seasonality of the eruption is important in defining the climate response (Kravitz and Robock, 2011; Marshall et al., 2021) and thus, a more pronounced response may have occurred where there is no coverage of paleoenvironmental proxies. For example, the ice core sulfate depositional signals and historic records suggest that the Hekla 1693 CE eruption occurred in February 1693 CE, with paleo-reanalysis data showing a pronounced cooling across Central Europe in spring 1693 CE (Fig. A.17a). Closer inspection of the records which are incorporated into the reanalysis show that this spring response is based on documentary evidence.

In contrast, summer (JJA) paleo-reanalysis data, which is dominated by tree-ring records, captures far less of this cooling signature (Fig. A17b). Therefore, historical documents, where available, with their monthly to seasonal resolution can help better explore the wider temporal climate responses to volcanic eruptions. However, the use of these records is not without limitations, owing to their poor spatial coverage (i.e., clustered in Europe). Ultimately, by identifying and incorporating records with a greater spatial and temporal coverage (i.e., sub-annual), the climate response to volcanic eruptions may be better assessed on a global and seasonal scale.

4. Conclusions

Following our geochemical attribution of the Greenland 1667 CE peak to the historic Tarumae (Shikotsu) eruption, we consider 1662 ±1 CE as the most likely date for the caldera-forming Long Island eruption, with 1654 ±1 CE as an alternative candidate. Both candidate dates are within existing radiocarbon constrained best age estimates for the date of the Long Island eruption (1651–1671 CE; 95.4 %). However, we tentatively use 1662 ±1 CE due to previous radiocarbon constraints suggesting a 68.2 % probability of occurrence between 1655 and 1665 CE. Future identification of tephra accompanying this peak in the polar ice cores would provide further confidence in this attribution. This differs from previous work, which suggested an age between 1665 and 1668 CE, thereby reaffirming the misalignment of South Pole ice-core records as previously identified by Sigl et al. (2014).

Through the geochemical attribution of the Tarumae eruption to 1667 CE within the polar ice-core records and the tentative assignment of the Long Island eruption to 1662 CE, we have revised volcanic sulfur emissions across the 17th century using a newly compiled dataset of sulfur from an array of ice cores from Antarctica and Greenland. Our revised VSSI estimates support the accuracy of ice core chronologies used within this work and agree well with global radiative forcing estimates.

Using paleoenvironmental proxies and a paleo-reanalysis dataset, we found that both the Long Island 1662 ±1 CE and Tarumae 1667 CE eruptions had limited climate impacts across the Northern Hemisphere and suggest that this may be a result of the low atmospheric sulfur loading after the tropical Long Island eruption and a larger tropospheric sulfate burden following the extratropical Tarumae eruption. These impacts contrast with the pronounced persistent (up to 3 years) Northern Hemisphere summer cooling following the four largest VSSIs across the study period (Mt. Parker, 1640 CE; unidentified event cluster, 1694 CE; Huaynaputina, 1600 CE; and Nevado del Ruiz, 1595 CE), with these responses agreeing well with previous studies. However, we recognise that there is a strong seasonal and spatial bias in the records used for assessing the climate impacts and emphasise a more representative global assessment would be possible through the availability of more high-resolution Southern Hemisphere records.

Finally, the attribution of Tarumae within the polar ice-core records has further constrained volcanic forcing during the Maunder Grand Solar Minimum. Ultimately, this may allow us to better understand the individual contributions of volcanic and solar forcing to climate change which may be explored through future climate model simulations.

CRediT authorship contribution statement

Imogen Gabriel: Writing – review & editing, Writing – original draft, Visualization, Methodology, Investigation, Formal analysis. **Helen M. Innes:** Writing – review & editing, Investigation. **Peter M. Abbott:** Writing – review & editing, Methodology, Investigation. **Jörg Franke:** Writing – review & editing, Resources. **Melanie Behrens:** Writing – review & editing, Investigation. **Nathan J. Chellman:** Writing – review & editing, Resources, Funding acquisition. **Maria Hörhold:** Writing – review & editing, Investigation. **William Hutchison:** Writing – review & editing, Investigation. **Joseph R. McConnell:** Writing – review & editing, Resources, Funding acquisition. **Birthe Twarloh:** Investigation. **Michael Sigl:** Conceptualization, Writing – review & editing, Writing – original draft, Visualization, Supervision, Methodology, Investigation, Formal analysis.

Funding sources

Imogen Gabriel, **Peter M. Abbott**, and **Michael Sigl** received funding from the European Research Council under the European Union's Horizon 2020 research and innovation programme (grant number: 820047). **Helen M. Innes** and **William Hutchison** are funded by a UKRI Future Leaders Fellowship (grant number: MR/S033505/1). The St Andrews EPMA facility is supported by the EPSRC (grant numbers: EP/T019298/1, EP/L017008/1, EP/R023751/1). **Jörg Franke** was funded by the European Research Council under the European Union's Horizon 2020 research and innovation programme (grant number: 787574). Collection and analysis of the Summit2023 core was supported by the US National Science Foundation (grant number: 2139293) to **Nathan J. Chellman and Joseph R. McConnell**. Development of the Greenland (Summit2015, TUNU2013, B19, NEEM-2011-S1) and Antarctic (WD, NUS, B40) continuous ice core sulfur and insoluble particle records was supported by the US National Science Foundation (grant numbers: 1406219, 1204176, 909541, 0538416, 0538427) to **Joseph R. McConnell**.

Declaration of competing interest

The authors declare that they have no known competing financial interests or personal relationships that could have appeared to influence the work reported in this paper.

Acknowledgements

We thank the NSF-Ice core facility (Denver, USA) for their hospitability and Chloe A. Brashear for her assistance when sampling the TUNU2013 ice core. Thanks to Sepp Kipfstuhl (AWI, Bremerhaven, Germany) for providing access to the B19 ice core. Thanks to the scientific consortia and funding agencies associated with NGRIP and EGRIP ice core drilling projects directed and organised by the Physics of Ice, Climate and Earth at the Niels Bohr Institute, Denmark. Thanks to Niklaus Bartlome, Richard Warren, and Noémie Wellinger for developing Climeapp, allowing visualisation of the ModE-RA climate paleoreanalysis data. Thanks to Pierre Lanari and Coralie Vesin for help with EPMA analysis at the University of Bern. We thank Russell Blong and two anonymous reviewers for their constructive feedback that helped improve the final version of the manuscript.

Appendix A. Supplementary data

Supplementary data to this article can be found online at https://doi.org/10.1016/j.jvolgeores.2025.108346.

Data availability

All data is provided with the manuscript.

References

Abbott, P.M., Plunkett, G., Corona, C., Chellman, N., McConnell, J.R., Pilcher, J.R., Stoffel, M., Sigl, M., 2021. Cryptotephra from the Icelandic Veiðivötn 1477 CE eruption in a Greenland ice core: confirming the dating of volcanic events in the 1450s CE and assessing the eruption's climatic impact. Clim. Past 17 (2), 565–585. https://doi.org/10.5194/cp-17-565-2021.

Abbott, P.M., McConnell, J.R., Chellman, N., Kipfstuhl, S., Hörhold, M., Freitag, J., Hutchison, W., Sigl, M., 2024. Mid-to Late Holocene East Antarctic ice-core tephrochronology: Implications for reconstructing volcanic eruptions and assessing their climatic impacts over the last 5,500 years. Quat. Sci. Rev. 329. https://doi.org/10.1016/j.quascirev.2024.108544.

Anchukaitis, K.J., Wilson, R., Briffa, K.R., Büntgen, U., Cook, E.R., D'Arrigo, R., Davi, N., Esper, J., Frank, D., Gunnarson, B.E., Hegerl, G., 2017. Last millennium Northern Hemisphere summer temperatures from tree rings: Part II, spatially resolved reconstruction. Quat. Sci. Rev. 163, 1–22. https://doi.org/10.1016/j.quascirev.2017.02.020.

Blong, R.J., 1982. The Time of Darkness: Local Legends and Volcanic Reality in Papua New Guinea. Australian National University Press, Canberra.

Blong, R.J., Kurbatov, A.V., 2020. Steps and missteps on the path to a 1665–1668 CE date for the VEI 6 eruption of Long Island, Papua New Guinea. J. Volcanol. Geotherm. Res. 395. https://doi.org/10.1016/j.jvolgeores.2020.106828.

Blong, R., Fallon, S., Wood, R., McKee, C., Chen, K., Magill, C., Barter, P., 2018. Significance and timing of the mid-17th-century eruption of Long Island, Papua New Guinea. The Holocene 28 (4), 529–544. https://doi.org/10.1177/09596836177355.

Brehm, N., Bayliss, A., Christl, M., Synal, H.A., Adolphi, F., Beer, J., Kromer, B., Muscheler, R., Solanki, S.K., Usoskin, I., Bleicher, N., 2021. Eleven-year solar cycles over the last millennium revealed by radiocarbon in tree rings. Nat. Geosci. 14 (1), 10–15. https://doi.org/10.1038/s41561-020-00674-0.

Budner, D., Cole-Dai, J., 2003. The Number and magnitude of large explosive volcanic eruptions between 904 and 1865 A.D.: Quantitative evidence from a New South Pole Ice Core. In: Robock, A., Oppenheimer, C. (Eds.), Volcanism and the Earth's Atmosphere, Eds. American Geophysical Union (AGU) Geophysical Monograph Series, Washington, D.C., pp. 165–176 https://doi.org/10.1029/139GM10

Burke, A., Moore, K.A., Sigl, M., Nita, D.C., McConnell, J.R., Adkins, J.F., 2019. Stratospheric eruptions from tropical and extra-tropical volcanoes constrained using high-resolution sulfur isotopes in ice cores. Earth Planet Sc Lett 521, 113–119. https://doi.org/10.1016/j.epsl.2019.06.006.

Burke, A., Innes, H.M., Crick, L., Anchukaitis, K.J., Byrne, M.P., Hutchison, W., McConnell, J.R., Moore, K.A., Rae, J.W., Sigl, M., Wilson, R., 2023. High sensitivity of summer temperatures to stratospheric sulfur loading from volcanoes in the Northern Hemisphere. Proc. Natl. Acad. Sci. USA 120. https://doi.org/10.1073/pnas.222181012.

Cole-Dai, J., 2010. Volcanoes and climate. WIRES. Clim. Chang. 1 (6), 824–839. https://doi.org/10.1002/wcc.76.

Cook, E., Abbott, P.M., Pearce, N.J., Mojtabavi, S., Svensson, A., Bourne, A.J., Rasmussen, S.O., Seierstad, I.K., Vinther, B.M., Harrison, J., Street, E., 2022. Volcanism and the Greenland ice cores: a new tephrochronological framework for the Last Glacial-Interglacial Transition (LGIT) based on cryptotephra deposits in three ice cores. Quat. Sci. Rev. 292, 107596. https://doi.org/10.1016/j.quascirev.2022.107596.

Coulter, S.E., Denham, T.P., Turney, C.S., Hall, V.A., 2009. The geochemical characterization and correlation of Late Holocene tephra layers at Ambra Crater and Kuk Swamp. Papua New Guinea. Geol J 44 (5), 568–592. https://doi.org/10.1002/gj.1164.

Crowley, T.J., Unterman, M.B., 2013. Technical details concerning development of a 1200 yr proxy index for global volcanism. Earth Syst. Sci. Data 5 (1), 187–197. https://doi.org/10.5194/essd-5-187-2013.

D'Arrigo, R., Klinger, P., Newfield, T., Rydval, M., Wilson, R., 2020. Complexity in crisis: the volcanic cold pulse of the 1690s and the consequences of Scotland's failure to cope. J. Volcanol. Geotherm. Res. 389. https://doi.org/10.1016/j.jvolgeores.2019.106746.

Davies, S.M., Albert, P.G., Bourne, A.J., Owen, S., Svensson, A., Bolton, M.S., Cook, E., Jensen, B.J., Jones, G., Ponomareva, V.V., Suzuki, T., 2024. Exploiting the Greenland volcanic ash repository to date caldera-forming eruptions and widespread isochrons during the Holocene. Quat. Sci. Rev. 334, 108707. https://doi.org/10.1016/j.quascirev.2024.108707.

De Silva, S.L., Zielinski, G.A., 1998. Global influence of the AD 1600 eruption of Huaynaputina, Peru. Nature 393, 455–458. https://doi.org/10.1038/30948.

Dunbar, N.W., Iverson, N.A., Van Eaton, A.R., Sigl, M., Alloway, B.V., Kurbatov, A.V., Mastin, L.G., McConnell, J.R., Wilson, C.J.N., 2017. New Zealand supereruption provides time marker for the Last Glacial Maximum in Antarctica. Sci. Rep. 7. https://doi.org/10.1038/s41598-017-11758-0.

Erhardt, T., Jensen, C.M., Adolphi, F., Kjær, H.A., Dallmayr, R., Twarloh, B., Behrens, M., Hirabayashi, M., Fukuda, K., Ogata, J., Burgay, F., 2023. High-resolution aerosol data from the top 3.8 kyr of the East Greenland Ice coring Project (EGRIP) ice core. Earth Syst. Sci. Data 15 (11), 5079–5091. https://doi.org/10.5194/essd-15-5079-2023.

Fang, S.W., Sigl, M., Toohey, M., Jungclaus, J., Zanchettin, D., Timmreck, C., 2023. The role of small to moderate volcanic eruptions in the early 19th century climate. Geophys. Res. Lett. 50 (22), e2023GL105307. https://doi.org/10.1029/2023GL105307.

Fei, J., Zhang, D.D., Lee, H.F., 2016. 1600 AD Huaynaputina eruption (Peru), abrupt cooling, and epidemics in China and Korea. Adv. Meteorol. 1, 3217038. https://doi.org/10.1155/2016/3217038.

Ferris, D.G., Cole-Dai, J., Reyes, A.R., Budner, D.M., 2011. South Pole ice core record of explosive volcanic eruptions in the first and second millennia A.D. and evidence of a large eruption in the tropics around 535 A.D. J. Geophys. Res.-Atmos. 116 (D17), 1–11. https://doi.org/10.1029/2011JD015916.

Fuglestvedt, H.F., Zhuo, Z., Toohey, M., Krüger, K., 2024. Volcanic forcing of high-latitude Northern Hemisphere eruptions. npj Clim. Atmos. Sci. 7 (1). https://doi.org/10.1038/s41612-023-00539-4.

Gabriel, I., Plunkett, G., Abbott, P.M., Behrens, M., Burke, A., Chellman, N., Cook, E., Fleitmann, D., Hörhold, M., Hutchison, W., McConnell, J.R., Oladottir, B.A., Preiser-Kapeller, J., Sliwinski, J.T., Sugden, P., Twarloh, B., Sigl, M., 2024. Decadal-to-centennial increases of volcanic aerosols from Iceland challenge the concept of a Medieval Quiet Period. Commun. Earth Env. 5, 194. https://doi.org/10.1038/s43247-024-01350-6.

Gabriel, I., Innes, H.M., Abbott, P.M., Hutchison, W., Chellman, N.J., Sigl, M., 2025a. Major oxide concentrations of individual glass tephra shards from the Greenland ice core TUNU2013_58.04-58.14m, Summit2023_180.52-108.69m, and Summit2023_108.22-108.37m samples [dataset]. PANGAEA. https://doi.org/10.1594/PANGAEA.974359.

Gabriel, I., Innes, H.M., Abbott, P.M., Hutchison, W., Chellman, N.J., Sigl, M., 2025b. Secondary standards for major oxide concentrations of individual glass tephra shards from the Greenland ice core TUNU2013_58.04-58.14m, Summit2023_180.52-108.69m, and Summit2023_108.22-108.37m samples [dataset]. PANGAEA. https://doi.org/10.1594/PANGAEA.974360.

Gao, C., Oman, L., Robock, A., Stenchikov, G.L., 2007. Atmospheric volcanic loading derived from bipolar ice cores: Accounting for the spatial distribution of volcanic deposition. J. Geophys. Res.-Atmos. 112 (D9). https://doi.org/10.1029/2006JD007461.

Gao, C., Robock, A., Ammann, C., 2008. Volcanic forcing of climate over the past 1500 years: an improved ice core-based index for climate models. J. Geophys. Res.-Atmos. 113 (D23). https://doi.org/10.1029/2008JD010239.

Global Volcanism Program, 2024. [Database] Volcanoes of the World (v. 5.1.6; 2 Mar 2024). Distributed by Smithsonian Institution, compiled by Venzke, E. https://doi.org/10.5479/si.GVP.VOTW5-2023.5.1 (accessed 2 March 2024).

Hall, M., Hayward, C., 2014. Preparation of micro- and crypto-tephras for quantitative microbeam analysis. Geol. Soc. Spec. Publ. 398, 21–28. https://doi.org/10.1144/SP398.5.

Hammer, C.U., Clausen, H.B., Dansgaard, W., 1980. Greenland ice sheet evidence of post-glacial volcanism and its climatic impact. Nature 288, 230–235. https://doi.org/10.1038/288230a0.

Hartman, L.H., Kurbatov, A.V., Winski, D.A., Cruz-Uribe, A.M., Davies, S.M., Dunbar, N.W., Iverson, N.A., Aydin, M., Fegyveresi, J.M., Ferris, D.G., Fudge, T.J., Osterberg, E.C., Hargreaves, G.M., Yates, M.G., 2019. Volcanic glass properties from 1459 C.E. volcanic event in South Pole ice core dismiss Kuwae caldera as a potential source. Sci. Rep. 9, 1–7. https://doi.org/10.1038/s41598-019-50939-x.

Haurwitz, M.W., Brier, G.W., 1981. A critique of the superposed epoch analysis method: its application to solar–weather relations. Mon. Weather Rev. 109, 2074–2079. https://doi.org/10.1175/1520-0493(1981)109<2074:ACOTSE>2.0.CO;2.

Hörhold, M., Münch, T., Weissbach, S., Kipfstuhl, S., Freitag, J., Sasgen, I., Lohmann, G., Vinther, B., Laepple, T., 2023. Modern temperatures in central-north Greenland warmest in past millennium. Nature 613, 503–507.

Hörhold, M., Twarloh, B., Behrens, M., Dallmayr, R., Erhardt, T., Meyer, H., 2025a. Anion Concentrations of the EGRIP Ice Core [dataset]. PANGAEA. https://doi.org/10.1594/PANGAEA.966041.

Hörhold, M., Twarloh, B., Behrens, M., Dallmayr, R., Erhardt, T., Meyer, H., 2025b. Cation Concentrations of the EGRIP Ice Core [dataset]. PANGAEA. https://doi.org/10.1594/PANGAEA.966039.

Huhtamaa, H., Helama, S., 2017. Distant impact: tropical volcanic eruptions and climate-driven agricultural crises in seventeenth-century Ostrobothnia, Finland. J. Hist. Geogr. 57, 40–51. https://doi.org/10.1016/j.jhg.2017.05.011.

Huhtamaa, H., Stoffel, M., Corona, C., 2022. Recession or resilience? Long-range socioeconomic consequences of the 17th century volcanic eruptions in northern Fennoscandia. Clim. Past 18 (9), 2077–2092. https://doi.org/10.5194/cp-18-2077-2022.

Hutchison, W., Gabriel, I., Plunkett, G., Burke, A., Sugden, P., Innes, H., Davies, S., Moreland, W.M., Krüger, K., Wilson, R., Vinther, B.M., Dahl-Jensen, D., Freitag, J., Oppenheimer, C., Chellman, N.J., Sigl, M., McConnell, J.R., 2024. High-Resolution Ice-Core analyses identify the Eldgjá eruption and a cluster of Icelandic and Trans-Continental tephras between 936 and 943 CE. J. Geophys. Res.-Atmos. 129 (16), e2023JD040142. https://doi.org/10.1029/2023JD040142.

Ilyinskaya, E., Mason, E., Wieser, P.E., Holland, L., Liu, E.J., Mather, T.A., Edmonds, M., Whitty, R.C.W., Elias, T., Nadeau, P.A., Schneider, D., McQuaid, J.B., Allen, S.E., Harvey, J., Oppenheimer, C., Kern, C., Damby, D., 2021. Rapid metal pollutant deposition from the volcanic plume of Kīlauea, Hawai'i. Commun. Earth Environ. 2, 1–15. https://doi.org/10.1038/s43247-021-00146-2.

Innes, H.M., Hutchison, W., Burke, A., 2024. Geochemical analysis of extremely fine-grained cryptotephra: new developments and recommended practices. Quat. Geochronol. 83. https://doi.org/10.1016/j.quageo.2024.101553.

Iverson, N.A., Kalteyer, D., Dunbar, N.W., Kurbatov, A., Yates, M., 2017. Advancements and best practices for analysis and correlation of tephra and cryptotephra in ice. Quat. Geochronol. 40, 45–55. https://doi.org/10.1016/j.quageo.2016.09.008.

Janebo, M.H., Thordarson, T., Houghton, B.F., Bonadonna, C., Larsen, G., Carey, R.J., 2016. Dispersal of key subplinian–Plinian tephras from Hekla volcano, Iceland: implications for eruption source parameters. B Volcanol 78 (66). https://doi.org/10.1007/s00445-016-1059-7.

Jensen, B.J.L., Pyne-O'Donnell, S., Plunkett, G., Froese, D.G., Hughes, P.D.M., Sigl, M., McConnell, J.R., Amesbury, M.J., Blackwell, P.G., van den Bogaard, C., Buck, C.E., Charman, D.J., Clague, J.J., Hall, V.A., Koch, J., Mackay, H., Mallon, G., McColl, L., Pilcher, J.R., 2014. Transatlantic distribution of the Alaskan White River Ash. Geology 42, 875–878. https://doi.org/10.1130/G35945.1.

Jochum, K.P., Willbold, M., Raczek, I., Stoll, B., Herwig, K., 2005. Chemical characterization of the USGS reference glasses GSA-1G, GSC-1G, GSD-1G, GSE-1G, BCR-2G, BHVO-2G and BIR-1G usig EPMA, ID-TIMS, ID-ICP-MS and LA-ICP-MS. Geostand. Geoanal. Res. 29, 285–302. https://doi.org/10.1111/j.1751-908X.2005.tb00901.x.

Jochum, K.P., Stoll, B., Herwig, K., Willbold, M., Hofmann, A.W., Amini, M., Aarburg, S., Abouchami, W., Hellebrand, E., Mocek, B., Raczek, I., 2006. MPI-DING reference glasses for in situ microanalysis: New reference values for element concentrations and isotope ratios. Geochem. Geophys. Geosyst. 7 (2). https://doi.org/10.1029/2005GC001060.

Jungclaus, J.H., Bard, E., Baroni, M., Braconnot, P., Cao, J., Chini, L.P., Egorova, T., Evans, M., Fidel González-Rouco, J., Goosse, H., Hurtt, G.C., Joos, F., Kaplan, J.O., Khodri, M., Klein Goldewijk, K., Krivova, N., Legrande, A.N., Lorenz, S.J., Luterbacher, J., Man, W., Maycock, A.C., Meinshausen, M., Moberg, A., Muscheler, R., Nehrbass-Ahles, C., Otto-Bliesner, B.I., Phipps, S.J., Pongratz, J., Rozanov, E., Schmidt, G.A., Schmidt, H., Schmutz, W., Schurer, A., Shapiro, A.I., Sigl, M., Smerdon, J.E., Solanki, S.K., Timmreck, C., Toohey, M., Usoskin, I.G., Wagner, S., Wu, C.J., Leng Yeo, K., Zanchettin, D., Zhang, Q., Zorita, E., 2017. The PMIP4 contribution to CMIP6 - Part 3: The last millennium, scientific objective, and experimental design for the PMIP4 past1000 simulations. Geosci. Model Dev. 10, 4005–4033. https://doi.org/10.5194/gmd-10-4005-2017.

Keegan, K.M., Albert, M.R., McConnell, J.R., Baker, I., 2014. Climate change and forest fires synergistically drive widespread melt events of the Greenland Ice Sheet. Proc. Natl. Acad. Sci. USA 111 (22), 7964–7967. https://doi.org/10.1073/pnas.1405397111.

Kravitz, B., Robock, A., 2011. Climate effects of high-latitude volcanic eruptions: Role of the time of year. J. Geophys. Res.-Atmos. 116 (D1). https://doi.org/10.1029/2010JD014448.

Kuehn, S.C., Froese, D.G., 2010. Tephra from Ice- A simple method to routinely mount, polish, and quantitatively analyze sparse fine particles. Microsc. Microanal. 16, 218–225. https://doi.org/10.1017/S1431927609991322.

Kuehn, S.C., Froese, D.G., Shane, P.A.R., 2011. The INTAV intercomparison of electron-beam microanalysis of glass by tephrochronology laboratories: Results and recommendations. Quartern Int. 246 (1–2), 19–47. https://doi.org/10.1016/j.quaint.2011.08.022.

Le Maitre, R.W., Streckeisen, A., Zanettin, B., Le Bas, M.J., Bonin, B., Bateman, P., Bellieni, G., Dudek, A., Efremova, S., Keller, J., Lamere, J., Sabine, P.A., Schmid, R., Sorensen, H., Woolley, A.R., 2002. Igneous Rocks: A Classification and Glossary of Terms, Recommendations of the International Union of Geological Sciences, Subcommission of the Systematics of Igneous Rocks. Cambridge University Press, Cambridge.

Lee, G., Burke, A., Hutchison, W., Sugden, P., Smith, C., McConnell, J.R., Sigl, M., Oppenheimer, C., Rasmussen, S.O., Steffensen, J.P., Lee, S.R., Ahn, J., 2024. Phasing and climate forcing potential of the Millennium Eruption of Mt. Baekdu, Commun Earth Environ 5. https://doi.org/10.1038/s43247-024-01713-z.

Legrand, M., 1997. Ice-core records of atmospheric sulphur. Philos. T R Soc. B 352, 241–250. https://doi.org/10.1098/rstb.1997.0019.

Luterbacher, J., Schmutz, C., Gyalistras, D., Xoplaki, E., Wanner, H., 1999. Reconstruction of monthly NAO and EU indices back to AD 1675. Geophys. Res. Lett. 26 (17), 2745–2748. https://doi.org/10.1029/1999GL900576.

Luterbacher, J., Xoplaki, E., Dietrich, D., Jones, P.D., Davies, T.D., Portis, D., Gonzalez-Rouco, J.F., Von Storch, H., Gyalistras, D., Casty, C., Wanner, H., 2001. Extending North Atlantic oscillation reconstructions back to 1500. Atmos. Sci. Lett. 2 (1–4), 114–124. https://doi.org/10.1006/asle.2002.0047.

Marshall, L., Johnson, J.S., Mann, G.W., Lee, L., Dhomse, S.S., Regayre, L., Yoshioka, M., Carslaw, K.S., Schmidt, A., 2019. Exploring how eruption source parameters affect volcanic radiative forcing using statistical emulation. J. Geophys. Res.-Atmos. 124 (2), 964–985. https://doi.org/10.1029/2018JD028675.

Marshall, L.R., Smith, C.J., Forster, P.M., Aubry, T.J., Andrews, T., Schmidt, A., 2020. Large variations in volcanic aerosol forcing efficiency due to eruption source parameters and rapid adjustments. Geophys. Res. Lett. 47 (19), e2020GL090241. https://doi.org/10.1029/2020GL090241.

Marshall, L.R., Schmidt, A., Johnson, J.S., Mann, G.W., Lee, L.A., Rigby, R., Carslaw, K.S., 2021. Unknown eruption source parameters cause large uncertainty in historical volcanic radiative forcing reconstructions. J. Geophys. Res.-Atmos. 126 (13), e2020JD033578. https://doi.org/10.1029/2020JD033578.

Maselli, O.J., Chellman, N.J., Grieman, M., Layman, L., McConnell, J.R., Pasteris, D., Rhodes, R.H., Saltzman, E., Sigl, M., 2017. Sea ice and pollution-modulated changes in Greenland ice core methanesulfonate and bromine. Clim. Past 13 (1), 39–59. https://doi.org/10.5194/cp-13-39-2017.

Mason, E., Edmonds, M., McConnell, J.R., 2022. Volatile trace metals deposited in ice as soluble volcanic aerosols during the 17.7.ka eruptions of Mt Takahe, West Antarctic Rift. Front. Earth Sci. 10. https://doi.org/10.3389/feart.2022.1002366.

McConnell, J., 2013. Ice core aerosol measurements in the Humboldt Ice Core [dataset]. Arctic Data Center. 10.18739/A23T9D689.

McConnell, J., 2016. Tunu, Greenland 2013 ice core chemistry [dataset]. Arctic Data Center. 10.18739/A2F18SF79.

McConnell, J.R., Sigl, M., Plunkett, G., Burke, A., Kim, W.M., Raible, C.C., Wilson, A.I., Manning, J.G., Ludlow, F., Chellman, N.J., Innes, H.M., Yang, Z., Larsen, J.F., Schaefer, J.R., Kipfstuhl, S., Mojtabavi, S., Wilhelms, F., Opel, T., Meyer, H., Steffensen, J.P., 2020. Extreme climate after massive eruption of Alaska's Okmok volcano in 43 bce and effects on the late roman republic and ptolemaic kingdom. Proc. Natl. Acad. Sci. USA 117, 15443–15449. https://doi.org/10.1073/pnas.2002722117.

McConnell, J.R., Chellman, N.J., Wensman, S.M., Plach, A., Stanish, C., Santibáñez, P.A., Brugger, S.O., Eckhardt, S., Freitag, J., Kipfstuhl, S., Stohl, A., 2024. Hemispheric-scale heavy metal pollution from South American and Australian mining and metallurgy during the Common Era. Sci. Total Environ. 912, 169431. https://doi.org/10.1016/j.scitotenv.2023.169431.

Moune, S., Gauthier, P.J., Gislason, S.R., Sigmarsson, O., 2006. Trace element degassing and enrichment in the eruptive plume of the 2000 eruption of Hekla volcano, Iceland. Geochim. Cosmochim. Acta 70, 461–479. https://doi.org/10.1016/j.gca.2005.09.011.

Nakagawa, M., Hiraga, N., Furukawa, R., 2011. Formation of a zoned magma chamber and its temporal evolution during the historic eruptive activity of Tarumai Volcano, Japan: Petrological implications for a long-term forecast of eruptive activity of an active volcano. J. Volcanol. Geotherm. Res. 205, 1–16. https://doi.org/10.1016/j.jvolgeores.2011.05.003.

Nakamura, Y., 2016. Stratigraphy, distribution, and petrographic properties of Holocene tephras in Hokkaido, northern Japan. Quat. Int. 397, 52–62. https://doi.org/10.1016/j.quaint.2015.07.056.

Namikawa, K., Ishikawa, Y., Sano, J., 1997. Stand dynamics during a 12-year period in a second-growth stand in a cool temperature forest in northern Japan. Ecol. Res. 12, 277–287. https://doi.org/10.1007/BF02529457.

Nardin, R., Amore, A., Becagli, S., Caiazzo, L., Frezzotti, M., Severi, M., Stenni, B., Traversi, R., 2020. Volcanic fluxes over the last millennium as recorded in the Gv7 Ice Core (Northern Victoria Land, Antarctica). Geosciences 10, 38. https://doi.org/10.3390/GEOSCIENCES10010038.

Neukom, R., Gergis, J., Karoly, D.J., Wanner, H., Curran, M., Elbert, J., González-Rouco, F., Linsley, B.K., Moy, A.D., Mundo, I., Raible, C.C., 2014. Inter-hemispheric temperature variability over the past millennium. Nat. Clim. Chang. 4, 362–367. https://doi.org/10.1038/nclimate2174.

Oka, S., Takaoka, S., 1996. A preliminary study on the effects of pyroclastic fall deposit on the forest ecosystem in southwestern Hokkaido, Japan. Geogr. Reports Tokyo Metrop. Univ. 31, 149–156.

Osman, M.B., Coats, S., Das, S.B., McConnell, J.R., Chellman, N., 2021. North Atlantic jet stream projections in the context of the past 1,250 years. Proc. Natl. Acad. Sci. USA 118 (38), e2104105118. https://doi.org/10.1073/pnas.2104105118.

PAGES2k Consortium, 2017. A global multiproxy database for temperature reconstructions of the Common. Era Sci Data 4, 170088. https://doi.org/10.1038/sdata.2017.88.

Pearson, C., Sigl, M., Burke, A., Davies, S., Kurbatov, A., Severi, M., Cole-Dai, J., Innes, H., Albert, P.G., Helmick, M., 2022. Geochemical ice-core constraints on the timing and climatic impact of Aniakchak II (1628 BCE) and Thera (Minoan) volcanic eruptions. PNAS Nexus 1, 1–12. https://doi.org/10.1093/pnasnexus/pgac048.

Pedersen, G., Montalvo, J., Einarsson, P., Vilmundardóttir, O.K., Sigurmundsson, F.S., Belart, J., Hjartardóttir, Á.R., Kizel, F., Rustowicz, R., Falco, N., Gísladóttir, G., 2018. Historical Lava Flow Fields at Hekla Volcano. South Iceland., Jökull, p. 68. https://hdl.handle.net/20.500.11815/968.

Piva, S.B., Barker, S.J., Iverson, N.A., Winton, V.H.L., Bertler, N.A., Sigl, M., Wilson, C.J., Dunbar, N.W., Kurbatov, A.V., Carter, L., Charlier, B.L., 2023. Volcanic glass from the 1.8 ka Taupō eruption (New Zealand) detected in Antarctic ice at~ 230 CE. Sci. Rep. 13. https://doi.org/10.1038/s41598-023-42602-3.

Plummer, C.T., Curran, M.A.J., Van Ommen, T.D., Rasmussen, S.O., Moy, A.D., Vance, T. R., Clausen, H.B., Vinther, B.M., Mayewski, P.A., 2012. An independently dated 2000-yr volcanic record from Law Dome, East Antarctica, including a new

perspective on the dating of the 1450s CE eruption of Kuwae, Vanuatu. Clim. Past 8 (6), 1929–1940. https://doi.org/10.5194/cp-8-1929-2012.
Plunkett, G., Sigl, M., Pilcher, J.R., McConnell, J.R., Chellman, N., Steffensen, J.P., Büntgen, U., 2020. Smoking guns and volcanic ash: The importance of sparse tephras in Greenland ice cores. Polar Res. 39. https://doi.org/10.33265/polar.v39.3511.
Plunkett, G., Sigl, M., McConnell, J.R., Pilcher, J.R., Chellman, N.J., 2023. The significance of volcanic ash in Greenland ice cores during the Common Era. Quat. Sci. Rev. 301, 107936. https://doi.org/10.1016/j.quascirev.2022.107936.
Ponomareva, V., Portnyagin, M., Pendea, I.F., Zelenin, E., Bourgeois, J., Pinegina, T., Kozhurin, A., 2017. A full Holocene tephrochronology for the Kamchatsky Peninsula region: applications from Kamchatka to North America. Quat. Sci. Rev. 168, 101–122. https://doi.org/10.1016/j.quascirev.2017.04.031.
Rasmussen, S.O., Dahl-Jensen, D., Fischer, H., Fuhrer, K., Hansen, S.B., Hansson, M., Hvidberg, C.S., Jonsell, U., Kipfstuhl, S., Ruth, U., Schwander, J., 2023. Ice-core data used for the construction of the Greenland Ice-Core Chronology 2005 and 2021 (GICC05 and GICC21). Earth Syst. Sci. Data 15 (8), 3351–3364. https://doi.org/10.5194/essd-15-3351-2023.
Robock, A., 2000. Volcanic eruptions and climate. Rev. Geophys. 38 (2), 191–219. https://doi.org/10.1029/1998RG000054.
Ruth, U., Wagenbach, D., Steffensen, J.P., Bigler, M., 2003. Continuous record of microparticle concentration and size distribution in the central Greenland NGRIP ice core during the last glacial period. J. Geophys. Res.-Atmos. 108 (D3), 1–12. https://doi.org/10.1029/2002jd002376.
Scaillet, B., Oppenheimer, C., 2024. On the budget and atmospheric fate of sulfur emissions from large volcanic eruptions. Geophys. Res. Lett. 51 (12), e2023GL107180. https://doi.org/10.1029/2023GL107180.
Schneider, L., Alloway, B.V., Blong, R.J., Hope, G.S., Fallon, S.J., Pain, C.F., Maher, W.A., Haberle, S.G., 2017. Stratigraphy, age and correlation of two widespread late Holocene tephras preserved within Lake Kutubu, Southern Highlands Province. Papua New Guinea. J Quaternary Sci 32 (6), 782–794. https://doi.org/10.1002/jqs.2959.
Schrod, J., Kleinhenz, D., Hörhold, M., Erhardt, T., Richter, S., Wilhelms, F., Fischer, H., Ebert, M., Twarloh, B., Della Lunga, D., Jensen, C.M., 2020. Ice-nucleating particle concentrations of the past: insights from a 600-year-old Greenland ice core. Atmos. Chem. Phys. 20, 12459–12482. https://doi.org/10.5194/acp-20-12459-2020.
Self, S., 1992. Krakatau revisited: the course of events and interpretation of the 1883 eruption. GeoJournal 28, 109–121. https://doi.org/10.1007/BF00177223.
Siggaard-Andersen, M.L., Steffensen, J.P., Fischer, H., 2002. Lithium in Greenland ice cores measured by ion chromatography. Ann. Glaciol. 35, 243–249. https://doi.org/10.3189/172756402781816483.
Siggaard-Andersen, M., Hansson, M.E., Steffensen, J.P., Jonsell, U., Rasmussen, S.O., 2022. NorthGRIP ice-core record of major ions measured using ion chromatography covering the last two millennia and additional short Holocene sections [dataset]. PANGAEA. https://doi.org/10.1594/PANGAEA.944172.
Sigl, M., McConnell, J.R., 2022. NEEM-2011-S1 ice-core aerosol record (conductivity, NH4, NO3, BC, acidity, Na, Mg, S, Ca, Mn, Sr, Ce) in NW-Greenland at 2 cm resolution from 86-1997 CE on the annual-layer counted NS1-2011 chronology [dataset]. PANGAEA. https://doi.org/10.1594/PANGAEA.940553.
Sigl, M., McConnell, J.R., Layman, L., Maselli, O., McGwire, K., Pasteris, D., Dahl-Jensen, D., Steffensen, J.P., Vinther, B., Edwards, R., Mulvaney, R., Kipfstuhl, S., 2013. A new bipolar ice core record of volcanism from WAIS Divide and NEEM and implications for climate forcing of the last 2000 years. J. Geophys. Res.-Atmos. 118, 1151–1169. https://doi.org/10.1029/2012JD018603.
Sigl, M., McConnell, J.R., Toohey, M., Curran, M., Das, S.B., Edwards, R., Isaksson, E., Kawamura, K., Kipfstuhl, S., Krüger, K., Layman, L., Maselli, O.J., Motizuki, Y., Motoyama, H., Pasteris, D.R., Severi, M., 2014. Insights from Antarctica on volcanic forcing during the Common Era. Nat. Clim. Chang. 4, 693–697. https://doi.org/10.1038/nclimate2293.
Sigl, M., Winstrup, M., McConnell, J.R., Welten, K.C., Plunkett, G., Ludlow, F., Büntgen, U., Caffee, M., Chellman, N., Dahl-Jensen, D., Fischer, H., Kipfstuhl, S., Kostick, C., Maselli, O.J., Mekhaldi, F., Mulvaney, R., Muscheler, R., Pasteris, D.R., Pilcher, J.R., Salzer, M., Schüpbach, S., Steffensen, J.P., Vinther, B.M., Woodruff, T. E., 2015. Timing and climate forcing of volcanic eruptions for the past 2,500 years. Nature 523, 543–549. https://doi.org/10.1038/nature14565.
Sigl, M., Fudge, T.J., Winstrup, M., Cole-Dai, J., Ferris, D., McConnell, J.R., Taylor, K.C., Welten, K.C., Woodruff, T.E., Adolphi, F., Bisiaux, M., 2016. The WAIS Divide deep ice core WD2014 chronology–Part 2: Annual-layer counting (0–31 ka BP). Clim. Past 12 (3), 769–786. https://doi.org/10.5194/cp-12-769-2016.
Sigl, M., Toohey, M., McConnell, J.R., Cole-Dai, J., Severi, M., 2022. Volcanic stratospheric sulfur injections and aerosol optical depth during the Holocene (past 11 500 years) from a bipolar ice-core array. Earth Syst. Sci. Data 14, 3167–3196. https://doi.org/10.5194/essd-14-3167-2022.
Sigl, M., McConnell, J.R., Chellman, N.J., Hörhold, M., Behrens, M., Twarloh, B., Gabriel, I., 2025a. Annual mean concentrations of (non-sea-salt) sulfur, non-sea salt chlorine, fluoride, insoluble particle concentrations from an array of 19 ice cores from Antarctica and seven ice cores from Greenland [dataset]. PANGAEA. https://doi.org/10.1594/PANGAEA.974172.
Sigl, M., McConnell, J., Chellman, N., Gabriel, I., 2025b. High time resolution records of sulfur and insoluble particle concentrations from five ice cores from Greenland and one from Antarctica between 1530 and 1710 CE and inferred volcanic contributions [dataset]. PANGAEA. https://doi.org/10.1594/PANGAEA.974177.
Sigvaldason, G.E., Óskarsson, N., 1986. Fluorine in basalts from Iceland. Contrib. Mineral. Petrol. 94, 263–271. https://doi.org/10.1007/BF00371435.
Smith, V.C., Costa, A., Aguirre-Díaz, G., Pedrazzi, D., Scifo, A., Plunkett, G., Poret, M., Tournigand, P.-Y., Miles, D., Dee, M.W., McConnell, J.R., Sunyé-Puchol, I., Dávila Harris, P., Sigl, M., Pilcher, J.R., Chellman, N., Gutiérrez, E., 2020. The magnitude and impact of the 431 CE Tierra Blanca Joven eruption of Ilopango, El Salvador. Proc. Natl Acad. Sci. USA 117 (42), 26061–26068. https://doi.org/10.1073/pnas.2003008117.
Stoffel, M., Corona, C., Ludlow, F., Sigl, M., Huhtamaa, H., Garnier, E., Helama, S., Guillet, S., Crampsie, A., Kleemann, K., Camenisch, C., McConnell, J., Gao, C., 2022. Climatic, weather, and socio-economic conditions corresponding to the mid-17th-century eruption cluster. Clim. Past 18 (5), 1083–1108. https://doi.org/10.5194/cp-18-1083-2022.
Sun, C., Plunkett, G., Liu, J., Zhao, H., Sigl, M., McConnell, J.R., Pilcher, J.R., Vinther, B., Steffensen, J.P., Hall, V., 2014. Ash from Changbaishan Millennium eruption recorded in Greenland ice: Implications for determining the eruption's timing and impact. Geophys. Res. Lett. 41, 694–701. https://doi.org/10.1002/2013GL058642.
Thomas, E., Vladimirova, D., Tetzner, D., 2022. CLIVASH2k Antarctic ice core chemistry database (Version 1.0) [dataset]. NERC EDS UK Polar Data Centre. https://doi.org/10.5285/9e0ed16e-f2ab-4372-8df3-fde7e388c9a7.
Thordarson, T., Larsen, G., 2007. Volcanism in Iceland in historical time: Volcano types, eruption styles and eruptive history. J. Geodyn. 43, 118–152. https://doi.org/10.1016/j.jog.2006.09.005.
Thornton, I.W.B., Cook, S., Edwards, J.S., Harrison, R.D., Schipper, C., Shanahan, M., Singadan, R., Yamuna, R., 2001. Colonization of an island volcano, Long Island, Papua New Guinea, and an emergent island, Motmot, in its caldera lake. VII. Overview and discussion. J. Biogeogr. 28 (11−12), 1389–1408. https://doi.org/10.1046/j.1365-2699.2001.2811121389.x.
Toohey, M., Sigl, M., 2017. Volcanic stratospheric sulfur injections and aerosol optical depth from 500 BCE to 1900 CE. Earth Syst. Sci. Data 9, 809–831. https://doi.org/10.5194/essd-9-809-2017.
Traufetter, F., Oerter, H., Fischer, H., Weller, R., Miller, H., 2004. Spatio-temporal variability in volcanic sulphate deposition over the past 2 kyr in snow pits and firn cores from Amundsenisen. Antarctica. J Glaciol 50 (168), 137–146. https://doi.org/10.3189/172756504781830222.
Valler, V., Franke, J., Brugnara, Y., Burgdorf, A.M., Lundstad, E., Hand, R., Samakinwa, E., Lipfert, L., Friedman, A.R., Brönnimann, S., 2023. ModE-RA - A global monthly paleo-reanalysis of the modern era (1421 to 2008): Set 1420-3_1850-1 [dataset]. World Data Center for Climate (WDCC) at DKRZ. 10.26050/WDCC/ModE-RA_s14203-18501.
Valler, V., Franke, J., Brugnara, Y., Samakinwa, E., Hand, R., Lundstad, E., Burgdorf, A. M., Lipfert, L., Friedman, A.R., Brönnimann, S., 2024. ModE-RA: a global monthly paleo-reanalysis of the modern era 1421 to 2008. Sci. Data 11, 36. https://doi.org/10.1038/s41597-023-02733-8.
Vinther, B.M., Clausen, H.B., Johnsen, S.J., Rasmussen, S.O., Andersen, K.K., Buchardt, S. L., Dahl-Jensen, D., Seierstad, I.K., Siggaard-Andersen, M.-L., Steffensen, J.P., Svensson, A., Olsen, J., Heinemeier, J., 2006. A synchronized dating of three Greenland ice cores throughout the Holocene. J. Geophys. Res.-Atmos. 111 (D13). https://doi.org/10.1029/2005JD006921.
Wanner, H., Pfister, C., Neukom, R., 2022. The variable European little ice age. Quat. Sci. Rev. 287. https://doi.org/10.1016/j.quascirev.2022.107531.
Warren, R., Bartlome, N.E., Wellinger, N., Franke, J., Hand, R., Brönnimann, S., Huhtamaa, H., 2024. ClimeApp: data processing tool for monthly, global climate data from the ModE-RA palaeo-reanalysis, 1422 to 2008 CE. Clim. Past 20, 2645–2662. https://doi.org/10.5194/cp-20-2645-2024.
Weierbach, H., LeGrande, A.N., Tsigaridis, K., 2023. The Impact of Background ENSO and NAO Conditions and Anomalies on the Modeled Response to Pinatubo-Sized Volcanic Forcing. Atmos. Chem. Phys. 23 (24), 15491–15505. https://doi.org/10.5194/acp-23-15491-2023.
Weißbach, S., Wegner, A., Opel, T., Oerter, H., Vinther, B.M., Kipfstuhl, S., 2016. Spatial and temporal oxygen isotope variability in northern Greenland–implications for a new climate record over the past millennium. Clim. Past 12 (2), 171–188. https://doi.org/10.5194/cp-12-171-2016.
White, S., Moreno-Chamarro, E., Zanchettin, D., Huhtamaa, H., Degroot, D., Stoffel, M., Corona, C., 2022. The 1600 CE Huaynaputina eruption as a possible trigger for persistent cooling in the North Atlantic region. Clim. Past 18, 739–757. https://doi.org/10.5194/cp-18-739-2022.
Wilson, R., Anchukaitis, K., Briffa, K.R., Büntgen, U., Cook, E., D'arrigo, R., Davi, N., Esper, J., Frank, D., Gunnarson, B., Hegerl, G., 2016. Last millennium northern hemisphere summer temperatures from tree rings: Part I: the long term context. Quat. Sci. Rev. 134, 1–18. https://doi.org/10.1016/j.quascirev.2015.12.005.
Winski, D.A., Fudge, T.J., Ferris, D., Osterberg, E.C., Fegyveresi, J.M., Cole-Dai, J., Thundercloud, Z., Cox, T.S., Kreutz, K.J., Ortman, N., Buizert, C., 2019. The SP19 chronology for the South Pole Ice Core–Part 1: volcanic matching and annual layer counting. Clim. Past 15 (5), 1793–1808. https://doi.org/10.5194/cp-15-1793-2019.
Zanchettin, D., Bothe, O., Graf, H.F., Lorenz, S.J., Luterbacher, J., Timmreck, C., Jungclaus, J.H., 2013. Background conditions influence the decadal climate response to strong volcanic eruptions. J. Geophys. Res.-Atmos. 118 (10), 4090–4106. https://doi.org/10.1002/jgrd.50229.
Zhu, F., Emile-Geay, J., Hakim, G.J., King, J., Anchukaitis, K.J., 2020. Resolving the differences in the simulated and Reconstructed Temperature Response to Volcanism. Geophys. Res. Lett. 47 (8), e2019GL086908. https://doi.org/10.1029/2019GL086908.